



Sensitivity of tropospheric chemical composition to halogen-radical chemistry using a fully coupled size-resolved multiphase chemistry–global climate system: halogen distributions, aerosol composition, and sensitivity of climate-relevant gases

M. S. Long¹, W. C. Keene², R. C. Easter³, R. Sander⁴, X. Liu⁵, A. Kerkweg⁶, and D. Erickson⁷

¹School of Engineering and Applied Sciences, Harvard University, Cambridge, MA, USA

²Department of Environmental Sciences, University of Virginia, Charlottesville, VA 22904, USA

³Atmospheric Sciences and Global Change Division, Pacific Northwest National Laboratory, Richland, Washington, USA

⁴Air Chemistry Department, Max-Planck Institute of Chemistry, 55020 Mainz, Germany

⁵Department of Atmospheric University of Wyoming, Laramie, WY 82071, USA

⁶Institute for Atmospheric Physics, University of Mainz, 55099 Mainz, Germany

⁷Computer Science and Mathematics Division, Oak Ridge National Laboratory, Oak Ridge, TN USA

Correspondence to: M. S. Long (mlong@seas.harvard.edu)

Received: 24 January 2013 – Published in Atmos. Chem. Phys. Discuss.: 7 March 2013

Revised: 3 February 2014 – Accepted: 5 February 2014 – Published: 7 April 2014

Abstract. Observations and model calculations indicate that highly non-linear multiphase atmospheric processes involving inorganic Cl and Br significantly impact tropospheric chemistry and composition, aerosol evolution, and radiative transfer. The sensitivity of global atmospheric chemistry to the production of marine aerosol and the associated activation and cycling of inorganic Cl and Br was investigated using a size-resolved multiphase coupled chemistry–global climate model (National Center for Atmospheric Research’s Community Atmosphere Model (CAM) v3.6.33). Simulated results revealed strong meridional and vertical gradients in Cl and Br species. They also point to possible physicochemical mechanisms that may account for several previously unexplained phenomena, including the enrichment of Br⁻ in submicron aerosol and the presence of a BrO maximum in the polar free troposphere. However, simulated total volatile inorganic Br mixing ratios in the troposphere were generally higher than observed, due in part to the overly efficient net production of BrCl. In addition, the emission scheme for marine aerosol and associated Br⁻, which is the only source for Br in the model, overestimates emission fluxes from the high-latitude Southern Ocean. Br in the stratosphere was lower than observed due to the lack of long-lived precursor organobromine species in the simulation. Comparing

simulations using chemical mechanisms with and without reactive Cl and Br species demonstrates a significant temporal and spatial sensitivity of primary atmospheric oxidants (O₃, HO_x, NO_x), CH₄, non-methane hydrocarbons (NMHCs), and dimethyl sulfide (DMS) to halogen cycling. Globally, halogen chemistry had relatively less impact on SO₂ and non-sea-salt (nss) SO₄²⁻ although significant regional differences were evident. Although variable geographically, much of this sensitivity is attributable to either over-vigorous activation of Br (primarily BrCl) via the chemical mechanism or overproduction of sea-salt aerosol simulated under higher-wind regimes. In regions where simulated mixing ratios of reactive Br and Cl fell within observed ranges, though, halogen chemistry drove large changes in oxidant fields and associated chemical processes relative to simulations with no halogens. However, the overall simulated impacts of Br chemistry globally are overestimated and thus caution is warranted in their interpretation.

1 Introduction

The development of comprehensive global Earth system models that are able to accurately simulate the climate system requires detailed understanding and treatment of multiphase atmospheric processes relevant to aerosol evolution and radiative transfer. However, due in part to limitations in computational power relative to numerical needs, most current Earth system models treat the physicochemical processing of size-resolved aerosols using parameterizations that are computationally conservative but, in many respects, inadequate to reliably characterize aerosol–climate interactions. These limitations contribute to the large uncertainties in the radiative effects of atmospheric aerosols, which are among the major factors that constrain our current understanding of and ability to predict global climate change.

Reliable simulation of the physical and chemical evolution of aerosols in the Community Earth System Model (CESM) and other Earth system models requires explicit evaluation of processes as a function of size. Because of direct physical feedbacks, representative simulation of climatic influences also requires an interactive online scheme for aerosol micro-physics and multiphase chemistry. A number of major issues must be considered to implement such a scheme (see Long et al., 2013).

The size- and composition-dependent properties of aerosols significantly influence radiative fluxes through the atmosphere via two sets of interrelated processes. First, aerosols scatter and absorb incident and outgoing radiation and thereby directly influence net radiative transfer through the atmosphere and the associated distribution and partitioning of heat (and related kinetic and thermodynamic properties). Second, aerosols act as cloud condensation nuclei (CCN) and thereby influence the microphysical properties of clouds including droplet number, size distribution, and lifetime. Through this latter set of processes, aerosols indirectly regulate radiative transfer via the associated modulation of physicochemical evolution and albedo of clouds. These processes also influence precipitation fields and, thus, the hydrologic cycle and related climatic feedbacks.

Aerosols also interact directly in the cycling and associated climatic effects of important tropospheric gases, particularly over the ocean. The production from marine-derived precursors and multiphase cycling of halogen radicals represents a significant net sink for ozone in the remote marine boundary layer (MBL) (Dickenson et al., 1999; Galbally et al., 2000; Nagao et al., 1999; Sander et al., 2003; Pszenny et al., 2004; Keene et al., 2009; Lawler et al., 2009, 2011; Saiz-Lopez, 2012) and a potentially important net source in polluted coastal (Tanaka et al., 2003; Osthoff et al., 2008) and continental air (Thornton et al., 2010). The associated formation and scavenging of halogen nitrates accelerates the conversion of NO_x to HNO_3 and particulate NO_3^- , thereby contributing to net O_3 destruction (Sander et al., 1999; Pszenny et al., 2004; Keene et al., 2009). Marine-derived halogen rad-

icals (BrO and atomic Cl) oxidize $(\text{CH}_3)_2\text{S}$ (dimethyl sulfide, DMS) in the gas phase (Toumi, 1994; Keene et al., 1996; Saiz-Lopez et al., 2004), and hypohalous acids oxidize S(IV) in aerosol solutions (Vogt et al., 1996; Keene et al., 1998; von Glasow et al., 2002; von Glasow and Crutzen, 2004). The large surface area of primary marine aerosols also competes with nuclear clusters (from gas-to-particle reactions) for condensable reaction products from the oxidation of gaseous precursors (including H_2SO_4 from SO_2 oxidation), thereby diminishing the potential for clusters to grow to sustainable size. Consequently, the climatic influences of sulfur cycling may be substantially less than predicted based on models that do not explicitly evaluate interactions involving primary marine aerosols (Quinn and Bates, 2011). Chlorine radicals also oxidize methane (an important greenhouse gas) (Platt et al., 2004; Lawler et al., 2009, 2011) and non-methane hydrocarbons (Keene et al., 2007; Pszenny et al., 2007), which leads to the production of organic compounds that may contribute to aerosol production and growth and, in the presence of sufficient NO_x , peroxy radicals that enhance oxidation potential. The photochemical processing of marine-derived organic compounds is an important in situ source of OH and other radicals that enhance oxidation potential within aerosol solutions (McDow et al., 1996; Anastasio and Newberg, 2007; Zhou et al., 2008).

In terms of mass flux, bursting bubbles produced by breaking waves at the ocean surface are the largest source of aerosols in Earth's atmosphere (Andreae and Rosenfeld, 2008). The nascent droplets dehydrate into equilibrium with ambient water vapor and undergo other rapid (seconds) multiphase transformations involving the scavenging of gases, aqueous and surface reactions, and volatilization of products. (e.g., Chameides and Stelson, 1992; Erickson et al., 1999; Sander et al., 2003). The sub- μm fractions dominate number concentrations in remote marine regions and their associated direct and indirect influences on radiative transfer and climate (e.g., O'Dowd et al., 1997).

Several previous 3-D modeling efforts have evaluated impacts of halogen cycling on climate-relevant atmospheric species. Von Glasow et al. (2004) simulated influences of Br radicals produced from the degradation of generic bromine-containing organic precursors on chemical processes in the troposphere. However, that study did not consider Br activated from marine aerosol, and, consequently, the authors characterized related consequences for photochemistry as lower limits. Yang et al. (2005) and Parrella et al. (2012) evaluated influences of inorganic Br originating from both marine aerosol and the photochemical degradation of organic precursors. Production from marine aerosol was based on the assumption that 50 % of the associated Br^- is activated. However, measurements indicate that Br^- deficits relative to conservative sea-salt constituents integrated over particle size distributions often exceed 50 % (e.g., Pszenny et al., 2004; Keene et al., 2009). In addition, these parameterization schemes do not consider radical recycling via

multiphase pathways other than HOBr + Br⁻ in acidic solution and BrNO₃ hydrolysis. In particular, the production and processing of ClNO₃ is an important sink for NO_x, thereby contributing to net O₃ destruction (Keene et al., 2009). Consequently, these studies may also underestimate the overall importance of Br chemistry. Saiz-Lopez et al. (2012) simulated impacts of Br, Cl, and I chemistry in the tropical marine troposphere based on the assumption that the rate-limiting step in halogen activation is the uptake of inorganic halogen species by aerosols. They utilized a parameterization based on uptake coefficients for Br, Cl, and I species and prescribed branching ratios for the associated production of halogen-atom precursors reported by Ordóñez et al. (2012). As acknowledged by Ordóñez et al. (2012), the reliability of this parameterization scheme is uncertain because it does not consider influences of important factors that regulate halogen activation and recycling, including solution acidity (e.g., Keene et al., 1998) and depletion of particulate-phase halides (e.g., Fickert et al., 1999). The sensitivity of model performance to this parameterization scheme was not reported. No previous 3-D modeling efforts have simulated impacts of inorganic Br cycling on tropospheric chemistry based on a process-level treatment of the underlying multiphase transformations that regulate the activation and cycling of inorganic halogens. To provide context for subsequent comparisons between results reported herein and those from the previous modeling efforts summarized above, major aspects of halogen-radical chemistry that were considered in each study are summarized in Table 1.

For this analysis, a comprehensive multiphase atmospheric chemistry mechanism was fully coupled with a microphysically enabled aerosol-size-resolving general circulation model. The sensitivity of global atmospheric chemistry to the production and associated activation and cycling of sea-salt derived inorganic Cl and Br was interpreted to evaluate performance of and diagnose limitations in the chemical mechanism. The sensitivity of the mechanism to boundary conditions – marine aerosol emissions in particular – is also discussed. We used a 3-mode size-resolving aerosol module (Modal Aerosol Module) version of the three-dimensional (3-D) National Center for Atmospheric Research's Community Atmosphere Model (CAM version 3.6.33; Gent et al., 2009; Liu et al., 2012; hereafter referred to as modal-CAM) coupled to the multiphase chemical module MECCA (Module Efficiently Calculating the Chemistry of the Atmosphere; Sander et al., 2005). This comprehensive chemical scheme explicitly evaluates the multiphase production and processing of inorganic Br and Cl. MECCA was implemented with minimal parameterization and tuning, thus permitting quantitative evaluation of limitations in the chemical mechanism. The companion paper by Long et al. (2013) describes the coupled modeling system and chemical mechanism in detail.

2 Model description

Atmospheric processes were simulated in 3-D using modal-CAM at $1.9^\circ \times 2.5^\circ$ lat–lon resolution with 26 vertical levels (Gent et al., 2009). Modal-CAM is a FORTRAN90 compliant general circulation system built upon an extensive set of high-performance computational routines to preserve scalability and performance of the model across changes in resolution and model physics.

The dynamical core (approximation of the equations of motion on a discrete, spherical grid) is based on a flux-form semi-Lagrangian method better suited for tracer transport. This approach permits grid-wide stability of the chemistry solution, in contrast to discrete methods that introduce large dispersion and diffusion errors in their approximation of the equations of motion which propagate into and destabilize the chemistry solver.

Modal-CAM incorporates a comprehensive set of processes that control the evolution and coupling of three fixed-width log-normally distributed aerosol modes (Aitken, accumulation and coarse). The modal aerosol treatment is described in detail in Liu et al. (2012). Each mode consists of internally mixed populations of non-sea-salt (nss) SO₄²⁻, organic matter from primary sources (OM), secondary organic aerosol (SOA) from volatile organic precursors, black carbon (BC), inorganic sea salt, and mineral dust. Nss SO₄²⁻ is assumed to be in the form of NH₄HSO₄. OM and BC are treated only in the accumulation mode. SOA is only in the Aitken and accumulation modes, and mineral dust is only in the accumulation and coarse modes. Aerosol number and aerosol water are also calculated for each mode. Aerosol mass and number associated with stratiform cloud droplets are treated explicitly

2.1 Marine aerosol source function

Size-resolved emissions of particle number, and inorganic sea-salt and OM mass from the surface ocean, were calculated in CAM as functions of wind speed and surface ocean chlorophyll *a* (chl *a*) based on Long et al. (2011). Modeled size bins were centered on 0.039, 0.076, 0.15, 0.52, 2.4, 4.9, 15.1 and 30 μm diameters at 98 % relative humidity (i.e., RH within the laminar sublayer immediately above the air–sea interface) across bin widths (dD_p) of 0.03, 0.05, 0.1, 0.2, 1.0, 3.0, 10.0 and 20.0 μm , respectively. Following dehydration to equilibrium water contents at an average RH of 80 % in the mixed layer above the laminar sublayer, compositions were summed over the three aerosol size modes considered by CAM. Since the 3-mode version of CAM considers OM mass only in the accumulation mode, the OM mass was summed over all particle sizes below 1.0 μm diameter at 80 % RH, and emitted directly into the accumulation mode (mode 1).

Table 1. Aspects of halogen-radical chemistry in the troposphere evaluated as part of this work and through previous 3-D modeling efforts.

Characteristic	von Glasow et al. (2004)	Yang et al. (2005)	Ordóñez et al. (2012)	Saiz-Lopez et al. (2012)	Parrella et al. (2012)	This work
Br Sources						
Sea-salt aerosol	–	Yes ²	Yes ³	Yes ³	Yes ⁴	Yes ⁵
Organic Br gases	Yes ¹	Yes	Yes	Yes	Yes	–
Sea ice	–	–	–	–	–	–
Strat./trop. exchange	Yes	Yes	Yes	Yes	Yes	–
Cl Sources						
Sea-salt aerosol	–	–	Yes ³	Yes ³	–	Yes ⁵
I sources						
Ocean surface	–	–	Yes ⁶	Yes ⁶	–	–
Organic I gases	–	–	Yes	Yes	–	–
NO _x oxidation						
via BrNO ₃	Yes	Yes	Yes	Yes	Yes	Yes
via ClNO ₃	–	–	Yes	Yes	–	Yes
Latitude (deg.)	90° N–90° S	90° N–90° S	90° N–90° S	30° N–30° S	90° N–90° S	90° N–90° S
Altitude range	Free trop.	Full trop.	Full trop.	Full trop.	Full trop.	Full trop.

¹Organic Br source tuned to match concentrations of inorganic Br in the free troposphere inferred from BrO measurements. ²Based on marine aerosol production functions from Monahan et al. (1986) and O'Dowd and Smith (1993) and the assumption that 50 % of associated Br⁺ is activated as Br₂. Percent debromination is constant at lower latitudes and varies seasonally at higher latitudes. ³Based on marine aerosol production function from Mahowald et al. (2006), the assumption that uptake of inorganic halogens by aerosols is the rate-limiting step in halogen activation, and prescribed branching ratios for associated production of halogen-radical precursors. ⁴Based on marine aerosol production function from Alexander (2005) and the same debromination scheme used by Yang et al. (2005). ⁵Based on marine aerosol production function from Long et al. (2011). ⁶Source of I₂ tuned to match measured IO in excess of that simulated from the degradation of organic I gases.

2.2 Prescribed conditions and initializations

CH₄, N₂O, and CO₂ mixing ratios were fixed at 1.77, 0.32, and 378 ppmv, respectively. O₃ was calculated online. Direct surface emissions of DMS, SO₂, SOA precursor gases, subgrid-scale NH₄HSO₄ (mode 1 and mode 2), NH₃, and NO_x were based on Dentener et al. (2006). Surface emissions of CO, CH₃OH, C₂H₄, C₃H₆, C₃H₈, and C₅H₈ (isoprene) were based on the Precursors of Ozone and their Effects in the Troposphere (POET) database for 2000 (Granier et al., 2005).

The atmosphere model was initialized at 1 January 2000. Due to the heavy computational burden of running the MECCA mechanism, and to reduce model spin-up time, the sea-surface temperature was based on offline data for the 2000 calendar year, and was cycled annually. The sea-ice interface used version 4 of the Community Sea Ice Model (CSIM4; Briegleb et al., 2004). The land interface used version 2 of the Community Land Model (CLM2; Dickinson et al., 2006). Fields of Chl *a* concentrations (in units of mg m⁻³) in surface seawater were set equal to monthly averages derived from SeaWiFS (Sea-viewing Wide Field-of-view Sensor) imagery (1° × 1°; Gregg, 2008) for the period September 1997 through December 2002, as in Long et al. (2011). The aerosol modes were initialized at zero number with sizes centered log-normally on 0.026, 0.11, and 2.0 µm

geometric mean dry diameters for the Aitken, accumulation, and coarse modes, respectively. The corresponding ranges for the log-normal centroids were 0.0087 to 0.052, 0.053 to 0.44, and 1.0 to 4.0 µm dry diameter, respectively.

2.3 Global simulations and reporting conventions

Results for the coupled MECCA scheme, for which chemical reactions involving halogens were calculated explicitly (denoted *Hal*), were compared with corresponding runs for which halogen chemistry was turned off (denoted *NoHal*). Differences in results were interpreted to evaluate the role of halogens in the physicochemical evolution of the model troposphere.

Unless otherwise noted, the following conventions are used. Values are based on grid-box area-weighted spatial fields for the simulated 10-year period from 1 January 2005 to 31 December 2014. Notation is specified for atmospheric region and time period over which statistics were calculated. Ten-year area-weighted statistics are referred to as ANN for annual, DJF for December/January/February, MAM for March/April/May, JJA for June/July/August, and SON for September/October/November. Spatial statistics for specific atmospheric regions were compiled over the Northern and Southern Hemisphere (NH and SH, respectively), the entire planetary boundary layer (PBL), the continental-only

boundary layer (CBL), marine-only boundary layer (MBL), and the entire free troposphere (FT). Model layers corresponding to these regions are defined below. Analyses based on specific model layers (e.g., the surface layer) are specified as such. Results for a given atmospheric spatial region are based on median and range of 10-year mean climatology for that region and time period (as defined above). For example, the annual O₃ mixing ratio for the planetary boundary layer (ANN PBL) would be reported as the median and range across the PBL of the 10-year climatological mean.

Temporal-only statistics for one grid box are reported as mean \pm standard deviation. For example, a simulated mixing ratio corresponding to a long-term measurement site is reported only as a 10-year climatological mean and standard deviation. When necessary to facilitate direct comparison with observations or results from other published simulations, simulated results are reported using the same convention as the reported values.

For all discussions here, the tropopause was defined as the minimum pressure level in the model (maximum altitude) above which the temperature lapse rate was positive (70.06 mb or \sim 18 km), which is consistent with the World Meteorological Organization's tropopause definition. In CAM, the boundary layer is not well resolved, and was therefore defined as the lowest four levels (highest pressure) of the model atmosphere (below an altitude corresponding to 867 mb). The free troposphere was defined as the region between the top of the boundary layer and the tropopause. For comparisons with measurements at surface sites for which altitudes are known, simulated results were interpolated vertically to the corresponding measurement altitudes. Otherwise, the results from the likely nearest model pressure level were used. Unless otherwise noted, comparisons between results for *Hal* relative to *NoHal* simulations are presented as percent deviation defined as (using O₃ as an example)

$$\% \text{ Deviation} (\text{O}_3) = \frac{[\text{O}_3]_{\text{Hal}} - [\text{O}_3]_{\text{NoHal}}}{[\text{O}_3]_{\text{NoHal}}} \times 100. \quad (1)$$

3 Results

3.1 Overview of comparisons with observations and previous model studies

Differences in the configurations for 3-D models of tropospheric halogen chemistry that have been developed to date contribute to significant variability in corresponding simulated results and their comparability with observations. In particular, none of these models incorporate the same set of halogen sources and multiphase processes (Table 1). All global models that evaluate processes involving marine aerosol incorporate different size-resolved aerosol production functions and corresponding size distributions that are uncertain by factors of about four (e.g., Lewis and Schwartz, 2004; Long et al., 2011). Differences in simulated produc-

tion fluxes of precursor halides and of aerosol surface area contribute to variability among modeled results. As noted in the Introduction, differences in the parameterization schemes for halogen activation and multiphase cycling involving marine aerosol also contribute to variability among results. It is evident from the above that unambiguous interpretation of causes for differences among simulated results based on these models is problematic. However, some generalizations are evident. Comparisons between simulated aerosol concentrations and aerosol optical depth (AOD) measured from satellites suggests that wind-speed-dependent production parameterizations for marine aerosol as employed in this and other global models of halogen chemistry may significantly overestimate aerosol production (by \sim 40 %) over the high-latitude Southern Ocean (Jaegle et al., 2011). This implies that all models may overestimate the corresponding simulated impacts of halogen chemistry on other atmospheric species in this region. We discuss this issue in more detail below. In addition, available evidence suggests that rates of inorganic Br activation and multiphase cycling as incorporated in the MECCA chemical mechanism overestimate rates in ambient marine air to some extent; causes for this divergence between simulations and observations are unknown (Keene et al., 2009; Sommariva and von Glasow, 2012). Consequently, simulated impacts of chemical processes involving Br that originates from marine aerosol reported herein should be considered upper limits. Because our model does not consider emissions and processing of longer-lived organic halogen-containing gases or exchange of reactive halogens with the stratosphere, overall simulated impacts of halogens in the upper troposphere reported herein are considered lower limits. Finally, our model does not consider important but poorly constrained chemical processes involving inorganic I-containing compounds or their associated impacts. Despite these limitations, our approach does represent the first process-level treatment of size-resolved multiphase chemical reactions involving sea-salt-derived Br and Cl-containing compounds in a global 3-D model. Results provide unique and important insight concerning the robustness and limitations of our current understanding of inorganic Cl and Br activation, as well as potential influences of marine aerosol production and processing on oxidation processes and the chemical evolution of climate-relevant species in the PBL and lower FT.

3.2 Marine aerosol population characteristics

Mean aerosol composition and mixing ratios of gases simulated for each atmospheric region are compiled in supplemental material (Tables S1 through S6). Globally averaged annual marine aerosol production flux, burden, dry and wet deposition for both the *Hal* and *NoHal* simulations (not shown, since these marine aerosol statistics were virtually identical to those for *Hal*) fell within the range of published estimates (Table 2). The total Na⁺ mass flux was

Table 2. Global annual mean Na^+ burden, production flux, lifetime, dry and wet deposition fluxes, and global median (and range) aerosol number concentration compared with published results based on other marine aerosol source functions. Uncertainties correspond to year-over-year standard deviation for the 10-year annual mean.

Study	Na^+ burden (Tg)	Na^+ source (10^3Tg y^{-1})	Na^+ lifetime (d)	Na^+ dry dep. (10^3Tg y^{-1})	Na^+ wet dep. (10^3Tg y^{-1})	Number conc. (cm^{-3})
<i>Hal</i> (this work)	2.5 ± 0.03	1.1 ± 0.02	0.86 ± 0.01	0.49 ± 0.01	0.56 ± 0.01	$266 (4.0 \times 10^0 - 4.4 \times 10^4)$
Clarke et al. (2006)	4.0	2.2	0.66	1.5	0.68	
O'dowd et al. (1997)	5.2	4.1	0.47	2.9	1.2	
Mårtensson et al. (2003)	0.55	1.7	1.2	0.061	0.11	
Monahan et al. (1986)	1.2	0.55	0.79	0.34	0.19	
Kerkweg et al. (2008)	2.4	1.7	0.5	0.76	0.90	
Textor et al. (2006)	2.4	1.6	0.5			

25 % less than that reported by Long et al. (2011), which resulted in part from differences in model physics between the different CAM versions used in the two studies (3.5.07 for Long et al. (2011) and 3.6.33 here) and the number of aerosol size bins considered (8 for Long et al. (2011) and 3 here). The corresponding spatial range in mean Na^+ lifetimes against deposition was also within that reported by Pierce and Adams (2006) of 0.46 to 2.72 days. Mean dry deposition fluxes are towards the lower end of published estimates, whereas wet fluxes fall near the mid-range of published estimates. Available evidence indicates that cloud and precipitation processes are represented reasonably well within CAM3 (e.g., Boville et al., 2006), which implies that simulated deposition fluxes are also reasonable.

3.3 Model sensitivity to inorganic halogen cycling

In the following text and tables, Br_t is defined as the sum of all volatile inorganic Br species, and Cl^* is defined as all inorganic Cl gases other than HCl , including HOCl , $2 \times \text{Cl}_2$, ClNO_2 , ClNO_3 , OCIO , and BrCl .

3.3.1 Br distributions

Simulated Br_t averaged over the tropospheric column ranged from 0.038 to 44 pmol mol^{-1} (median $6.1 \text{ pmol mol}^{-1}$), and those for ANN-FT ranged from 0.038 to 32 pmol mol^{-1} (median $2.5 \text{ pmol mol}^{-1}$). Based on Br sources other than sea-salt debromination, von Glasow et al. (2004) reported Br_t in the FT ranging from 1 to 6 pmol mol^{-1} , which brackets the median value for our *Hal* simulation. Based on prescribed debromination of marine aerosol, photolysis of organic precursors, and exchange with the stratosphere, Parrella et al. (2012) simulated a mean tropospheric Br_t mixing ratio of $3.2 \text{ pmol mol}^{-1}$, which is about two times lower than the median value for our simulation. This relatively lower mean is driven in part by (1) constraining Br activation based on aerosol debromination to percentages that are lower than those simulated by the full MECCA scheme and also lower than many measured values (e.g., Pszenny et al., 2004; Keene et al., 2009) and (2) not considering net destruction of NO_x

and O_3 driven by the formation and processing of ClNO_3 , which box model calculations suggest can account for greater than 50 % of the total heterogeneous NO_x sink in both polluted and clean marine air (e.g., Keene et al., 2009).

Simulated zonal median Br_t reveals little Br_t in the upper FT and stratosphere, which is inconsistent with observation (e.g., Fitznerberger et al., 2000; see Supplement Fig. S1) and model calculations (von Glasow et al., 2004). Most stratospheric Br is believed to originate from the photolysis of long-lived organic Br species (e.g., CH_3Br) (Montzka et al., 2003), which are not considered in the MECCA chemical mechanism employed for these simulations or the emission fields for Modal-CAM. Offline Br sources would have been required to achieve observed levels of stratospheric Br_t with the computational resources available for this analysis. The radiative transfer scheme used to calculate photochemical rates was tuned to reproduce stratospheric O_3 climatological means. Consequently, the impact of Br in the upper troposphere on rates of tropospheric photochemistry is believed to be negligible.

With one exception, simulated Br_t was higher than the few available observations (Table 3). For Hawaii, the excess simulated Br_t is driven in part by the emission of volcanic SO_2 at the surface rather than at an appropriate altitude within the model, which accelerates aerosol acidification, thereby driving non-representative halogen activation from larger, short-lived marine aerosol. Regions of the eastern North and South Atlantic Ocean in Table 3 are associated with large gradients in NO_x that constrain the reliability of comparisons between observations and model simulations. In addition, as mentioned above, excess sea-salt aerosol and limitations in the MECCA scheme tend to overpredict ambient mixing ratios of volatile reactive Br. This is discussed in detail in Sect. 4.

Global median vertical profiles and speciation of Br_t for ANN and JJA (Fig. 1) reveal that, between the surface and 700 to 800 mb pressure level (2 to 3 km altitude), Br_t is dominated by roughly equal amounts of Br_2 and BrCl on a molecular basis. For DJF, BrCl was higher than Br_2 by a factor of about two. At higher altitudes, HBr(g) (most of which is produced via the reaction of $\text{Br} + \text{HCHO}$) increases to become

Table 3. Median (and range) for total volatile Br (Br_t ; pmol mol $^{-1}$) measured at Hawaii (Pszenny et al., 2004) and along a transect through the eastern North and South Atlantic oceans (Keene et al., 2009) and simulated Br_t and BrCl for the surface layer within the corresponding grid cells. Reported median and ranges for simulated Br_t and BrCl along the transect are based on a box bounded by the north–south/east–west limits of the transect segment, as reported in Keene et al. (2009).

Location and time	Measured Br_t	Simulated Br_t	Simulated BrCl
Hawaii (21° N, 158° W; Sep 1999)	3.7 (< 2–9)	22.7 (19.6–23.4)	10.3 (9.0–11.7)
NE Atlantic (43–51° N, 2° E–10° W; Oct 2003)	7.2 (3.1–12.3)	17.5 (2.3–63.9)	6.7 (0.4–23.2)
NE Atlantic (10–33° N, 14–20° W; Oct–Nov 2003)	18.8 (8.2–30.1)	14.5 (7.2–29.5)	2.7 (0.0–14.9)
E Atlantic (1–10° N, 13–20° W; Nov 2003)	2.4 (< 0.1–3.1)	12.7 (8.5–22.2)	6.0 (2.9–10.2)
SE Atlantic (1° N–18° S, 4° E–13° W; Nov 2003)	6.2 (4.4–10.1)	17.5 (0.1–44.4)	6.0 (0–15.7)

the dominant gas-phase Br species, whereas, in the lower troposphere, HBr(g) is efficiently scavenged by liquid aerosol or cloud droplets. In the FT, most Br is recycled in the gas phase via



with an important secondary pathway (ranging from 5 to 20 % of the total atomic Br source) through

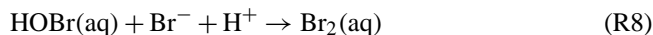


In the NH FT, $\text{BrO} + \text{NO} \rightarrow \text{Br} + \text{NO}_2$ competes with Reaction (R3) to recycle Br at approximately equal proportions as the effect of Reactions (R3) and (R4) together.

In the mid- and high-latitude FT, 7 to 15 % of available HOBr is converted to BrCl via the multiphase pathway involving accumulation mode aerosol:



In the MBL, 15 to 50 % of HOBr reacts via the above pathway. The reactions



and photolysis of BrCl and Br_2 generate atomic Br (and Cl), completing the autocatalytic cycle initiated by Reaction (R1).

Br enrichments, defined as Br^- to Na^+ ratio in excess of that found in seawater, in sub- μm aerosol have been observed throughout the MBL (e.g., Sander et al., 2003), but until now models have been unable to explain them. For example, in the CAABA box model, MECCA chemistry predicts efficient activation of particulate Br^- in all aerosol size fractions (e.g., Keene et al., 2009) and, thus, no significant Br enrichment of marine aerosol within the MBL. The *Hal* simulation produced these enrichments, driven by cycling of Br species between the PBL and FT. In the model, relatively insoluble forms of Br_t are detrained from the MBL and accumulate in the FT, whereas most of the highly soluble parent aerosol is largely confined to the MBL. Simulated Br cycling in the FT leads to enrichments in particulate Br relative to inorganic sea salt (i.e., $\text{EF(Br)} > 1$) throughout most of the FT (see Supplement Tables S1 and S2). Br accumulates in FT aerosols via two principal pathways:

1. Secondary Br^- is formed via the oxidation of aqueous SO_2 (in the form of HSO_3^- and SO_3^{2-}) by HOBr.
2. HBr(g) condenses onto newly formed and preexisting aerosol.

The subsequent transport and entrainment of condensed or condensable reaction products back into the PBL accounts for the Br enrichment of sub- μm aerosol size fractions measured within the PBL. The role of this dynamic process is evident in a slight but statistically significant ($p < 0.10$) negative correlation between HBr(g) and model vertical velocity (not shown). Within the PBL, the incorporation of secondary Br^- into fine-mode particles formed via nucleation, and subsequent coagulation into accumulation-mode particles likely affects EF(Br) across the size distribution as well. However, since the model does not distinguish between fresh and aged aerosols, the relative contributions of different pathways to simulated EF(Br) in the PBL cannot be quantified explicitly.

While Br continuously cycles through the aerosol population even in environments with low aerosol liquid water content, the equilibration with HBr(g) dominates the net Br exchange, leading to steady-state enrichments of the smaller

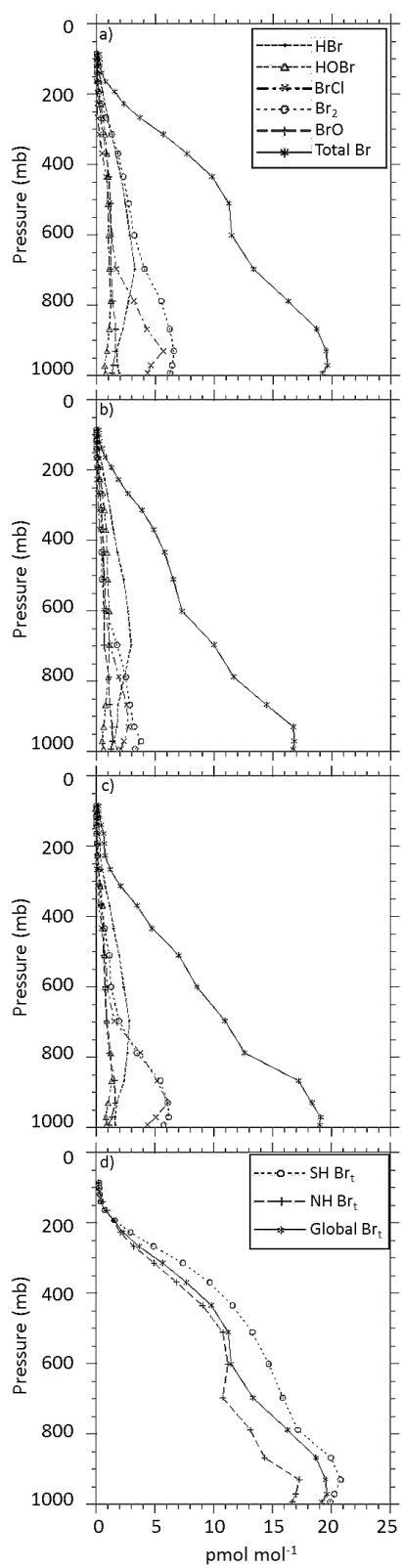


Fig. 1. Spatial median vertical profiles of Br_t and its component gases for (a) ANN, (b) JJA, and (c) DJF; (d) ANN Br_t for NH, SH and global regions.

(yet relatively more abundant at altitude) aerosols. Both the zonal median EF(Br) for bulk aerosol in the model surface layer and available measurements of EF(Br) (taken from Sander et al., 2003) indicate a slight NH latitudinal gradient at high latitudes, which is more pronounced in the observations (Fig. 2). Sander et al. (2003) suggest that the EF(Br) greater than unity in the NH may result from anthropogenic Br emissions in the region (primarily the North Sea and Scandinavia) leading to bulk enrichments. While zonal averages are not directly comparable to individual observations, the model suggests a stronger latitudinal trend in the SH. This is likely due to the strong subsidence in the high latitudes, consistent with the hypothesized mechanism of fine aerosol enrichment observed throughout the marine boundary layer. Sparse measurements in that region provide limited information with which to evaluate the simulated pattern. Geographically and seasonally coincident comparisons between simulated and measured EF(Br) for size-resolved marine aerosol indicate strong agreement (Fig. 3g–i).

Simulations suggest that Br originating from marine aerosol debromination at lower latitudes may contribute to reactive Br species over polar regions. For example, a persistent but seasonally variable maximum in simulated BrO ranging from 3 to 4 pmol mol⁻¹ was evident in the FT around 500 to 600 mb extending from approximately 60° S southward to the pole. This feature was driven by the transport of Br_t from the MBL across a band from 40° S to 20° S into the FT, southward, leading to the subsequent production and recycling of BrO, HOBr, and Br₂ via multiphase pathways detailed above. While comparison to O₃ mixing ratios suggests that Br mixing ratios are overpredicted in the SH troposphere, Br cycling pathways in the FT would likely sustain similar transport-driven patterns at lower Br_t abundance.

Vertically integrated simulated tropospheric BrO in polar regions over the 10-year period (Fig. 4) ranged from 0.011×10^{13} to $4.9 \times 10^{13} \text{ cm}^{-2}$ (within the range simulated by von Glasow et al., 2004). Simulated median BrO column burdens were 0.56×10^{13} , 0.97×10^{13} , 0.58×10^{13} and $0.85 \times 10^{13} \text{ cm}^{-2}$ for DJF, MAM, JJA and SON periods, respectively. Corresponding median PBL BrO mixing ratios were 1.1, 2.3, 1.5 and 1.5 pmol mol⁻¹ for DJF, MAM, JJA, and SON, respectively. Median FT BrO was 0.15, 0.20, 0.25 and 0.33 pmol mol⁻¹ for DJF, MAM, JJA and SON, respectively. Maximum column-integrated BrO for the MAM NH was $4.9 \times 10^{13} \text{ cm}^{-2}$, which is similar to the maximum tropospheric column burden of $3.9 (\pm 2.5) \times 10^{13} \text{ cm}^{-2}$ estimated based on profiles measured from aircraft over the Arctic during springtime (Salawitch et al., 2010). Typical NH springtime peak total column burdens measured by the Ozone Monitoring Instrument (OMI) aboard NASA's Aura satellite (e.g., Richter et al., 2002) exceed maximum simulated values by a factor of ~2. These springtime peaks (referred to as "bromine explosions") typically occur over polar ice caps in association with the activation of Br from brine films on surfaces of ice or snow and frost flows (Simpson et

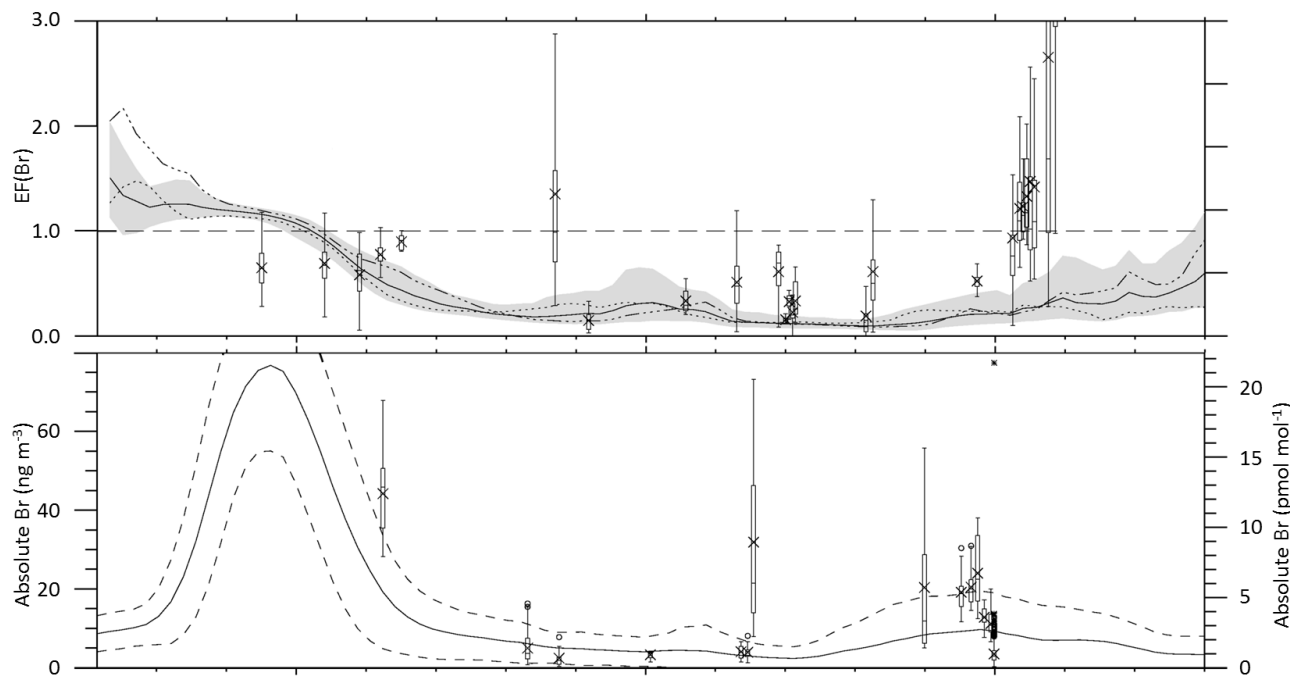


Fig. 2. Simulated zonal (a) EF(Br) and (b) absolute Br⁻ concentration in the model surface layer, and the corresponding measurement values reported by Sander et al. (2003) and Keene et al. (2009). Boxes and whiskers indicate minimum, 25th-quartile, median, 75th-quartile and maximum values. Crosses indicate means. In (a), simulated media are indicated by the solid line, the shaded area depicts 25–75th quartile range, the dash-dotted line depicts the JJA median, and the dotted line depicts the DJF median. The horizontal dashed line indicates unity (i.e., no enrichment or depletion relative to conservative sea-salt species). In (b) simulated media are indicated by the solid line, 25th and 75th quartiles by the dashed lines, and maxima and minima by the dotted lines.

al., 2007; Piot and von Glasow, 2008); these Br sources are not considered in our model. High mixing ratios of BrO in the FT during these periods have been attributed primarily to lofting of reactive Br produced at the surface via vigorous convection over ice leads driven by warm exposed water (Salawitch et al., 2010). Although our simulated results probably overestimate BrO and thus cannot be interpreted quantitatively relative to measurements, the presence of sea-salt-derived Br species over the model poles in the absence of local sources suggests that transport from lower latitudes may contribute to BrO in both the PBL and FT in these regions during springtime.

Simulated BrO for May and June across all 10 years at Summit, Greenland, ranged from 0.9 to 3.5 pmol mol⁻¹. To estimate daytime mean mixing ratios from the monthly mean data, we assumed that BrO mixing ratios dropped to zero at night and scaled the monthly mean value by the ratio of daylight to nighttime hours per the time of year and latitude. The daylight-adjusted mixing ratios are within the range of observed BrO (1 to 5 pmol mol⁻¹) at that location during spring, which is attributed primarily to snow chemistry (Stutz et al., 2011). Simulated BrO over Greenland is controlled by a combination of downwelling from the FT and subsequent activation of HBr(g), which again implies that sea-salt-derived Br species may contribute to the observed BrO.

A subset of available BrO measurements in the MBL is compared with the corresponding simulated values in Table 4. The modeled mixing ratios are averaged over diel cycles and adjusted to daytime values as described above. Simulated daytime mixing ratios agreed with observations within a factor of about two to three at all locations. The simulated BrO maxima in the tropical Atlantic and Pacific MBL (Fig. 5) have not been probed via direct measurement. But, as was the case with simulated Br_t, circulation and the coarse model resolution constrain the reliability of comparisons between measurements and simulated results in regions of strong chemical gradients. For example, mean BrO in grid boxes immediately to the east of that corresponding to São Vicente, Cape Verde, were a factor of two lower than that reported in Table 4.

The spatial median mixing ratio for simulated BrO in the tropics (including factor of two accounting for day/night ratio in the tropics) was 2.7 (5×10^{-3} – 9.7; mean: 2.9) pmol mol⁻¹ for the PBL and 0.14 (2×10^{-3} – 6.8 pmol mol⁻¹; mean: 0.53) pmol mol⁻¹ for the FT. These results are consistent with ship-based observations less than or equal to 3.6 pmol mol⁻¹ as reported by Saiz-Lopez et al. (2012). Saiz-Lopez et al. (2012) simulated BrO for the tropics ranging from 0.5 to 2 pmol mol⁻¹. Differences in results based on these two modeling studies are driven in

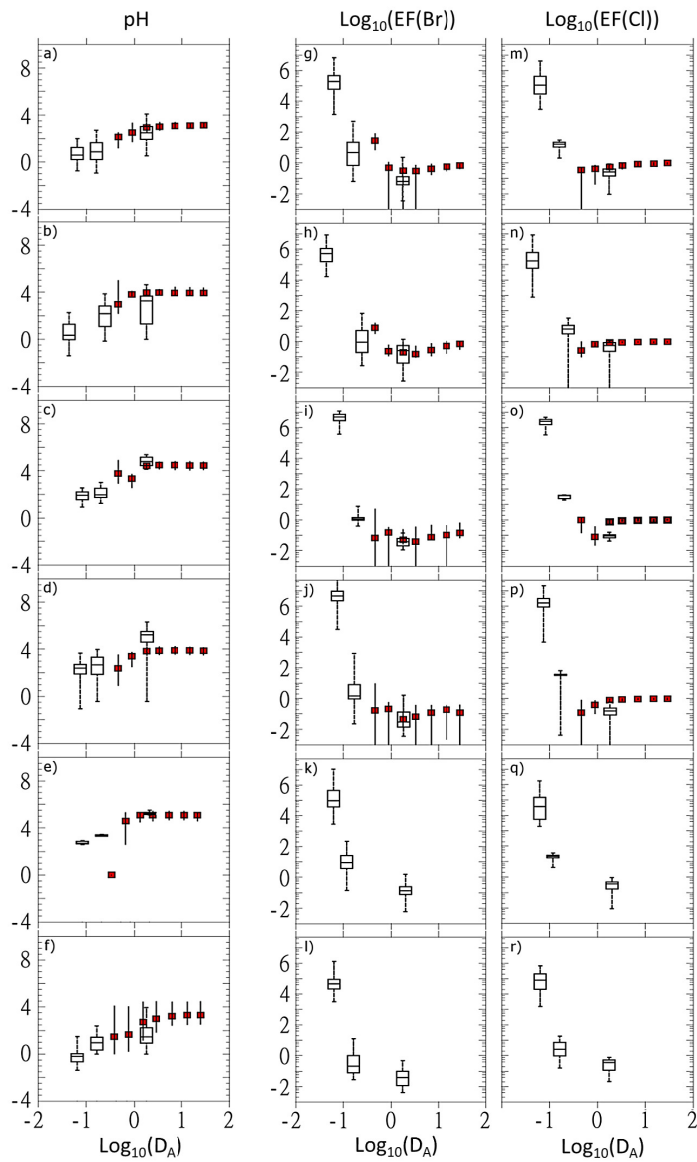


Fig. 3. Size-resolved (**a–f**) pH inferred from measurements, and, where available, (**g–l**) measured EF(Br) and (**m–r**) EF(Cl), in black line with red filling, and the corresponding values simulated with *Hal* in black line with open box. Boxes and whiskers depict maximum, 75th-quartile, median, 25th-quartile, and minimum values. D_A is the ambient particle diameter in μm . The top four rows correspond to the regions in the eastern North and South Atlantic oceans reported by Keene et al. (2009): row 1 is EURO, 2 is NAFR, 3 is ITCZ, and 4 is SATL. Row 5 corresponds to Hawaii (Pszenny et al., 2004), and row 6 corresponds to the New England Air Quality Study (NEAQS) along the US east coast (Keene et al., 2004).

part by the different Br activation and recycling mechanisms discussed above (Table 1). Our simulations for the tropics yield a median equivalent vertical column of approximately $0.7 \times 10^{13} \text{ cm}^{-2}$ for the PBL, $0.7 \times 10^{12} \text{ cm}^{-2}$ for the FT, and 0.53×10^{13} (0.04×10^{13} – 1.3×10^{13}) cm^{-2} for the total tropospheric column burden. The simulated column burden is less than the $1.5 \times 10^{13} \text{ cm}^{-2}$ based on satellite observations reported by Theys et al. (2011). Since the range was not reported by Theys et al. (2011) it is difficult to evaluate the

satellite vertical columns relative to the range in our simulated results.

Throughout most of the lower troposphere and boundary layer, the $\text{BrO} + \text{NO}$ reaction is the largest source of atomic Br (Table 5). The exception is the southern MBL where $\text{BrO} + \text{BrO}$, and HOBr and Br_2 photolysis dominate. In the global free troposphere simulated atomic Br originates primarily from $\text{BrO} + \text{NO}$ and HOBr photolysis in approximately equal proportions. The dominant sources

Table 4. Measured and simulated mean BrO mixing ratios (pmol mol^{-1}) \pm standard deviations (when available) for sites reported by Sander et al. (2003; Table 5) and Read et al. (2008). Simulated results are based on 10-year temporal means for the surface layer during the sampling month and within the grid box corresponding to the measurements.

Location and time	Measured	Simulated ^b	Day / night ^c	Est. daytime mean ^d
Hawaii (20° N, 155° W; Sep 1999)	<2	2.1 \pm 0.20	1.96	4.1 \pm 0.39
Finokalia, Crete (35° N, 26° E; Jul–Aug 2000)	<0.7–1.5	0.072 \pm 0.040	1.68	0.12 \pm 0.067
Made Head, Ireland (53° N, 10° W; Apr–May 1997)	1.1–2.5	1.1 \pm 0.41	1.60	1.8 \pm 0.66
Made Head, Ireland (53° N, 10° W; Sep–Oct 1998)	<1	0.96 \pm 0.49	2.04	2.0 \pm 1.0
Tenerife, Canary Islands (29° N, 17° W; Jun–Jul 1997)	3	2.9 \pm 0.53	1.71	5.0 \pm 0.91
Weybourne, Great Britain (53° N, 1° E; Oct 1996)	<2	0.018 \pm 0.006	2.29	0.041 \pm 0.014
São Vicente, Cape Verde (17° N, 25° W; Oct 2006–Oct 2007)	2.5 \pm 1.1 ^a	2.9 \pm 0.93	1.98	5.7 \pm 1.8

^aMaximum daytime values reported by Read et al. (2008). Nighttime values were below detection limits (0.5–1.0 pmol mol^{-1}). ^bSimulated values are based on averages of monthly-mean data as output by CAM. ^cSince the simulated results are based on monthly means, and assuming BrO is close to zero during nighttime, the ratio of daylight hours to nighttime hours at the specified location and time is used to scale to a daytime BrO mean value. ^dEstimated daytime mean is the simulated mean multiplied by the day / night factor as described in footnote c

Table 5. Percentage contribution of different production pathways for atomic Br vs. sum of all pathways based on ANN climatological means for different regions of the atmosphere.

	PBL	FT	Trop.	NH CBL	SH CBL	NH MBL	SH MBL
$\text{BrO} + \text{NO} \rightarrow \text{Br} + \text{NO}_2$	22 %	30 %	26 %	61 %	54 %	27 %	12 %
$\text{HOBr} + h\nu \rightarrow \text{Br} + \text{OH}$	12 %	27 %	19 %	5.6 %	7 %	9 %	12 %
$\text{BrCl} + h\nu \rightarrow \text{Br} + \text{Cl}$	18 %	8.5 %	14 %	9.9 %	9.2 %	23 %	15 %
$\text{Br}_2 + h\nu \rightarrow \text{Br} + \text{Br}$	18 %	11 %	15 %	18 %	21 %	17 %	21 %
$\text{BrO} + \text{BrO} \rightarrow 2 \text{Br} + \text{O}_2$	15 %	11 %	13 %	3.0 %	5.9 %	8.4 %	23 %
$\text{BrO} + \text{ClO} \rightarrow \text{Br} + \text{OCIO}$	5.0 %	5.8 %	5.3 %	1.0 %	0.4 %	5.4 %	3.3 %
$\text{BrO} + \text{ClO} \rightarrow \text{Br} + \text{Cl} + \text{O}_2$	4.3 %	4.9 %	4.4 %	0.8 %	0.4 %	4.8 %	2.9 %
$\text{BrO} + \text{DMS} \rightarrow \text{DMSO} + \text{Br}$	2.9 %	0.3 %	1.8 %	0.1 %	0.5 %	3.2 %	8.0 %
$\text{BrO} + \text{CH}_3\text{O}_2 \rightarrow \text{Br} + \text{HCHO} + \text{HO}_2$	2.0 %	1.0 %	1.6 %	0.4 %	0.4 %	2.1 %	2.1 %
$\text{BrNO}_2 + h\nu \rightarrow \text{Br} + \text{NO}_2$	0.0 %	0.0 %	0.0 %	0.4 %	0.3 %	0.0 %	0.0 %

for simulated HOBr in the free troposphere are $\text{BrO} + \text{HO}_2$ (84 %) and $\text{BrO} + \text{CH}_3\text{O}_2$ (16 %; primarily from CH_4 oxidation). As the result of low liquid water content, Br radicals in the free troposphere recycle primarily in the gas phase; although as discussed above, heterogeneous recycling is also important.

3.3.2 Cl Distributions

Simulated HCl mixing ratios fell within the ranges of most available measurements in the MBL. For example, HCl measured along a transect in the eastern Atlantic MBL was 682 (106 to 1404) pmol mol^{-1} in the vicinity of the European continent, 348 (91 to 746) pmol mol^{-1} adjacent to northern Africa, 82 (<23 to 207) pmol mol^{-1} in the Intertropical Convergence Zone, and 267 (81 to 453) pmol mol^{-1} adjacent to southern Africa (Keene et al., 2009). Corresponding simulated median surface HCl mixing ratios for these regions were 352 (8 to 1577), 906 (271 to 1914), 424 (294 to 697), and 445 (0.11 to 3155) pmol mol^{-1} , respectively. Maximum HCl mixing ratios in the eastern Atlantic were generally coincident with acid-displacement reactions involving HNO_3 in

marine regions downwind of major NO_x emission sources. As for Br_t , the strong gradients along the cruise track constrain the reliability of comparisons between measured and simulated HCl. Pszenny et al. (2004) measured HCl ranging from <30 to 250 pmol mol^{-1} (mean, 100 pmol mol^{-1}) in on-shore flow within the Hawaiian MBL, whereas the corresponding simulated surface median is 1247 (1046 to 1383) pmol mol^{-1} . These high simulated values at Hawaii reflect acidification of marine aerosol by local volcanic SO_2 emissions, which were emitted at the model surface. For comparison, simulated HCl upwind of the volcanic SO_2 plume was more than a factor of two lower.

Differences between aerosol pH in *Hal* vs. *NoHal* simulations reflect the influence of HCl-phase partitioning on aerosol solution acidity. Acid displacement of HCl by HNO_3 and other relatively more soluble acids that accumulated as marine aerosols age transfers acidity from the aerosol solution to the gas phase and thereby sustains higher solution pHs in the *Hal* simulation. Conversely, in *NoHal*, Cl is chemically inert, HCl does not volatilize as aerosols acidify with age, and, thus, acidity associated with condensed acids accumulates in the aerosol, resulting in relatively lower pHs

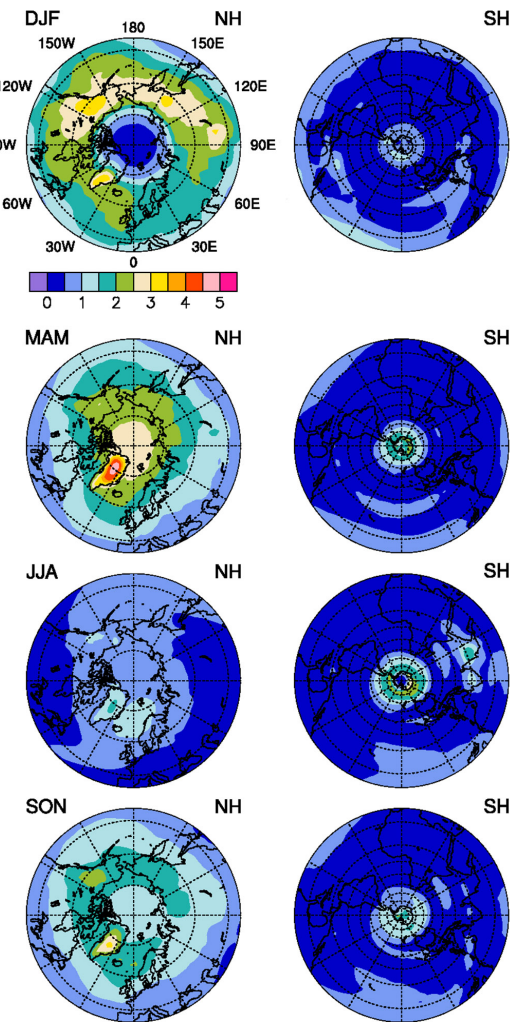


Fig. 4. Vertically integrated tropospheric BrO (10^{13} cm^{-2}) for the northern and southern hemispheric (NH, SH) polar regions, averaged over winter (DJF), spring (MAM; March/April/May), summer (JJA), and fall (SON).

(not shown). For all locations at which published estimates of aerosol pH based on in situ observations were available, simulated pHs based on *Hal* (Fig. 3a–f) compared better with those estimates than did pHs based on *NoHal* (not shown; also see Keene et al., 2009).

Simulated Cl* mixing ratios in the PBL are higher over much of the NH high latitudes, relative to other regions, with peak values in marine-influenced air downwind of major population and industrial regions. This is due to interactions with anthropogenic NO_x emissions (see Sect. 3.3.3). Simulated Cl* in the SH MBL (ranging from less than 0.01 to 340 pmol mol⁻¹, median 27 pmol mol⁻¹) was comprised of 46, 16, 6 and 1 % BrCl, Cl₂ (on an atomic basis), HOCl, and ClNO₂, respectively, based on median values. Cl* in the NH MBL was comprised of 20, 29, 3 and 10 % BrCl, Cl₂, HOCl, and ClNO₂, respectively, based on median values. In

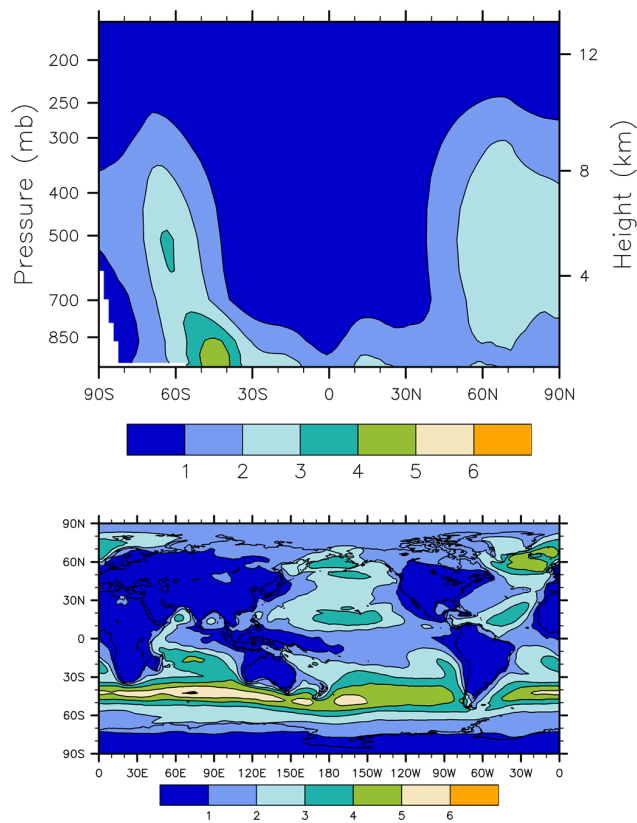
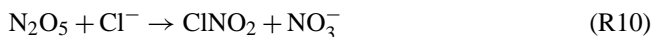


Fig. 5. Annual mean (a) zonal and (b) PBL BrO mixing ratios (pmol mol⁻¹).

contrast, over NH continents, ClNO₂ made up 69 % of Cl* and was higher than ClNO₂ in the NH MBL by a factor of 10 (see Supplement Table S4). This reflects the differences in NO_x loadings between both continental and marine troposphere, and the Southern and Northern Hemisphere. In the MECCA chemical mechanism, ClNO₂ is produced at night and subsequently photolyzes following sunrise via



Significant production is limited to highly polluted conditions with NO_x mixing ratios greater than $\sim 1 \text{ nmol mol}^{-1}$. ClNO₂ cycling is important in oxidation processes over coastal and continental regions (e.g., Ostroff et al., 2008; Simon et al. 2009, Thornton et al., 2010; Phillips et al., 2012; Brown et al., 2013). Mean simulated ClNO₂ mixing ratios in the summertime surface layer adjacent to the US Texas Gulf Coast were $134 (\pm 51) \text{ pmol mol}^{-1}$ (not adjusted for diel cycling) and were consistent both with observations made by Osthoff et al. (2008) and non-polluted simulation results (Simon et al., 2009). Mean simulated ClNO₂ mixing ratios for February at Boulder, CO, USA ($40^\circ \text{ N } 105^\circ \text{ W}$), were

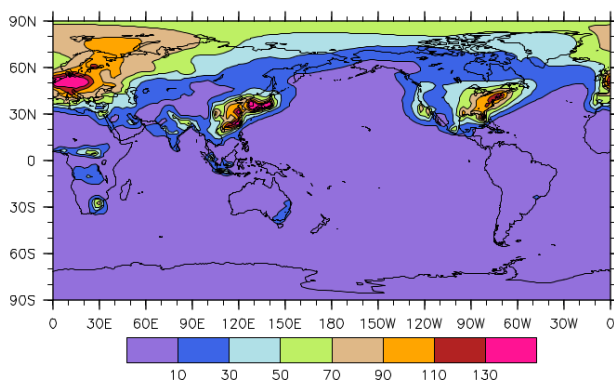


Fig. 6. ANN-PBL CINO_2 mixing ratio (pmol mol^{-1}).

129 (± 38) pmol mol^{-1} , which is within the ranges of CINO_2 mixing ratios observed by Thornton et al. (2010; less than 1 to 210 pmol mol^{-1}) and Brown et al. (2013; less than 1 to 1300 pmol mol^{-1}). The simulated distribution of CINO_2 over North America (Fig. 6) is also generally consistent with production patterns based on the GEOS-Chem model (Thornton et al., 2010). In all cases, the condensation of HCl sustained CINO_2 production when Cl^- concentrations were low over inland continental regions, consistent with recent observations (Young et al., 2013). CINO_2 mixing ratios simulated by *Hal* are generally higher and extend over broader geographic regions downwind from continents relative to those simulated by Erickson et al. (1999), and compare well with limited observations. During a March–April 2008 cruise in the North Atlantic, Kercher et al. (2009) report nighttime CINO_2 mixing ratios from 100 to 250 pmol mol^{-1} within the Long Island Sound (coordinates not reported; assumed in the vicinity of 41.5° N, 70° W), and at or near 25 to 50 pmol mol^{-1} further offshore (45° N, 55° W). Simulated CINO_2 mixing ratios within the corresponding grid cells, which like BrO were adjusted by the daylight-to-nighttime ratio, reflecting the season- and latitude-adjusted ratio of daytime to nighttime were 302 (± 88.4) and 75.6 (± 36.3) pmol mol^{-1} , respectively. The broad distribution of CINO_2 in the high latitudes suggests that its transport and cycling is important as a source for atomic Cl and a nocturnal reservoir for NO_x in polluted continental and marine regions.

Simulated atomic Cl in the global MBL ranged from 0 to $8.4 \times 10^4 \text{ cm}^{-3}$, which brackets reported values inferred from measurements of NMHCs and C_2Cl_4 (0 to $\sim 10^5 \text{ cm}^{-3}$; Rudolph et al., 1996; Singh et al., 1996). The simulated atomic Cl concentration of $2.6 \pm 1.5 \times 10^4 \text{ cm}^{-3}$ in New England (USA) coast air during summer was within the corresponding range of estimates based on relative concentration changes in NMHCs (2×10^4 to $6 \times 10^4 \text{ cm}^{-3}$; Pszenny et al., 2007). An estimate of $3.3 \pm 1.1 \times 10^4 \text{ cm}^{-3}$ derived from measurements made during a North Atlantic cruise in June 1992 (Wingenter et al., 1996), was similar to a simulated value of $4.8 \pm 1.6 \times 10^4 \text{ cm}^{-3}$ for the same region.

Measurements in the Southern Ocean MBL yielded estimated atomic Cl concentrations of $720 \pm 100 \text{ cm}^{-3}$, which is a factor of two lower than our simulated summertime surface mean of $2.0 \pm 1.6 \times 10^3 \text{ cm}^{-3}$ (Wingenter et al., 1999). The ANN-SH-MBL median for simulated values ($3.5 \times 10^3 \text{ cm}^{-3}$) was within the estimated 0.26×10^4 to $1.8 \times 10^4 \text{ cm}^{-3}$ required to sustain observed CH_4 isotope ratios in the southern MBL (Allan et al., 2011; Platt et al., 2004).

Using a similar chemical mechanism and associated observations, Lawler et al. (2009, 2011) investigated Cl speciation in detail at the Cape Verde Atmospheric Observatory (17° N, 25° W). Our results, averaged over May and June for the 10-year period, were similar to the clean case reported by Lawler et al. (2009) and the base and low-acid cases reported in Lawler et al. (2011): our average HNO_3 , O_3 , and NO_x were $34.5 (\pm 7.9)$, $24.8 (\pm 2.5)$ and $55.7 (\pm 12.1) \text{ pmol mol}^{-1}$, respectively. Cl, HOCl, Cl_2 and HCl were $3.6 (\pm 1.0) \times 10^5 \text{ cm}^{-3}$, $15.8 (\pm 4.4)$, $2.4 (\pm 1.2)$, and $683 (\pm 210) \text{ pmol mol}^{-1}$, respectively. Our simulated HCl is relatively higher than, but within the range of, their observations for the unpolluted MBL. Cl_2 (multiplied by a factor of two to account for diel cycling in the tropics) in our simulations was between the new source and ns + low-acid cases in Lawler et al. (2011). Our simulated atomic Cl is higher than that simulated by Lawler et al. (2009 – clean case; 2011 – base case), but its dominant source in our model is BrCl photolysis. Lawler et al. (2009) measured no BrCl above the estimated detection limit of 2 pmol mol^{-1} but report a simulated BrCl mixing ratio of 4 pmol mol^{-1} . In contrast, our median simulated mixing ratio for this grid cell was $17.9 (\pm 3.1) \text{ pmol mol}^{-1}$. The large gradients in this region probably contributed to the divergence in these simulated results based on a similar chemical mechanism. Neither measured nor simulated BrCl was reported by Lawler et al. (2011).

We note that, unless otherwise indicated, model output is based on monthly averages that do not reflect daytime maxima, and thus peak mixing ratios for species produced photochemically in ambient air are higher. In addition, the simulation did not consider non-marine sources for Cl in the atmosphere, and thus the total production fluxes and burdens of Cl should be considered lower limits.

3.4 Impact of halogens on O_3 , OH, HO_2 and NO_x

Comparisons between simulated and observed mixing ratios of chemical constituents with which halogens are directly coupled provide relevant insight concerning multiphase halogen chemistry as described by MECCA. In this section, we focus on the primary atmospheric oxidants O_3 , OH, HO_2 and NO_x and their roles in and sensitivity to Cl and Br cycling.

3.4.1 O₃

Deviations between the *Hal* and *NoHal* simulations of temporally averaged surface O₃ (Fig. 7) and the corresponding zonal-median vertical distribution fields (see Supplement Fig. S3) reveal less O₃ globally in the *Hal* simulation. These results are driven primarily by (1) the direct destruction of O₃ via reaction with halogen radicals (Table 6) and (2) the net reduction in O₃ production resulting from the accelerated oxidation of NO_x via formation and processing of halogen nitrates (discussed in more detail below; Sander et al., 1999; Pszenny et al., 2004; Keene et al., 2009). While Reaction (R1) destroys ozone directly (Fig. 8a), null cycles initiated by the subsequent reactions



reduce net O₃ destruction via Reaction (R1). In the PBL specifically, Reaction (R12) reduced the net impact of Reaction (R1) by a median of 4.7 % (0.3–73.1 %) primarily over land and in proximity to major NO_x sources (Fig. 8b). Reaction (R13) reduced the net O₃ destruction by 71 % (6.4–87.0) primarily in the MBL. Reaction (R14) (not shown) was everywhere < 1 %. The result was that, considering the null cycles, the net impact of atomic Br on O₃ destruction was less than predicted by considering Reaction (R1) alone (Fig. 8d; Table 6).

The largest absolute deviations were in the SH high latitudes and generally coincident with relatively greater sea-salt emissions and associated Br activation and O₃ destruction (Fig. 7c). Large deviations in the NH high latitudes were driven primarily by the over-vigorous production of BrCl (see above) and associated O₃ destruction. The reduction of NO_x and its influence on O₃ was also significant in the free troposphere with a similar latitudinal pattern (mean deviation of –39 %; not shown). These results are not consistent with those from previous studies in two respects. First, the geographic distribution of Br-mediated O₃ loss is different. In our study, the negative ozone deviations in high-latitude MBL and polar PBL are coincident with high sea-salt concentrations (in both *Hal* and *NoHal*), and NO and lower HO₂ concentrations (see Sect. 3.3.2) relative to the *NoHal* simulations, which enhanced O₃ destruction via the NO + O₃ reaction path. In regions where NO abundance decreased from *NoHal* to *Hal* (e.g., in the remote tropical MBL) the net O₃ loss was also lower. Second, overall ozone loss is greater in our simulations. Saiz-Lopez et al. (2012) calculate net O₃ loss due to halogens from 6 to 20 % in the tropical troposphere. Our results exceed 20 % for most of the tropical MBL

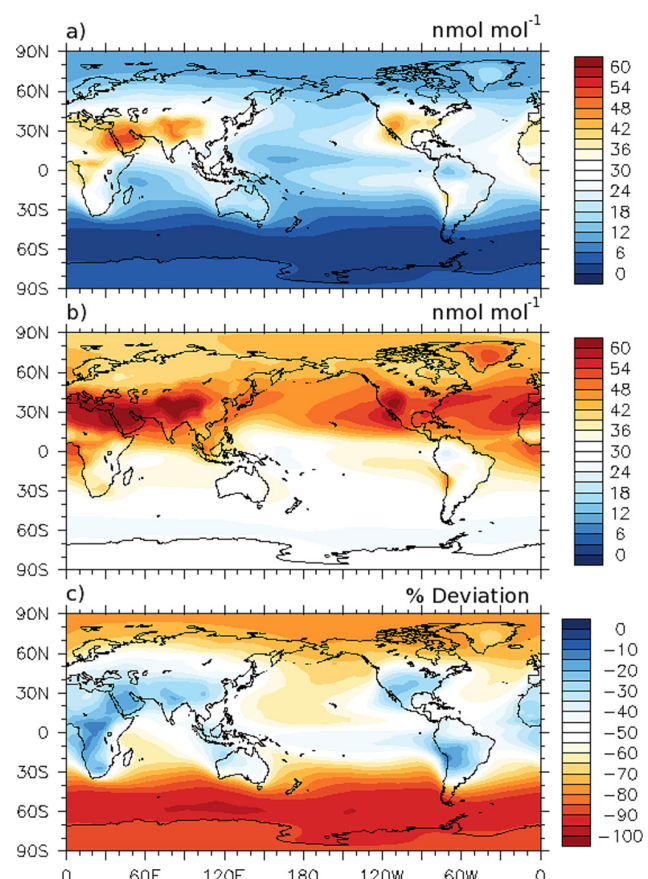


Fig. 7. ANN-PBL O₃ (nmol mol⁻¹) for (a) *Hal* and (b) *NoHal*, and (c) the corresponding percent deviations.

and are around 15 to 20 % for the tropical FT. Differences in the treatment of Br activation in the two models (Table 1) contribute to variability in the corresponding simulated O₃.

In addition, the suppression of RO₂ production by BrO leads to a net decrease in RO₂ mixing ratios in the PBL. This suppressed the reaction of NO + RO₂ globally by 38 and 49 % in the PBL and FT, respectively, thereby contributing to net O₃ destruction.

O₃ simulated with *Hal* and *NoHal* is compared with O₃ measured in near-surface air at Hawaii during September (Pszenny et al., 2004) and along a transect through the eastern Atlantic during October and November (Keene et al., 2009) in Fig. 9. Relative to *NoHal*, the *Hal* simulations yielded O₃ mixing ratios that were closer to those observed in all cases.

Annual mean O₃ mixing ratios for World Ozone and Ultraviolet Radiation Data Centre (WOUDC) sites (Table 7) are compared to corresponding simulated O₃ mixing ratios in the PBL and in the FT at the 500 mb pressure level in Fig. 10. Red markers indicate stations in the SH PBL. Relative to mean mixing ratios measured in the PBL and 500 mb levels, deviations in mean (\pm standard deviation) O₃ simulated

Table 6. Relative contributions of different pathways to total direct O₃ destruction in *Hal* and in *NoHal* simulations and the corresponding total O₃ destruction via all pathways in *Hal* relative to *NoHal* simulations expressed as percentages; based on ANN means for different regions of the atmosphere.

	PBL	FT	NH CBL	SH CBL	NH MBL	SH MBL
<i>Hal</i>						
$R_{O_3+h\nu}/ R_{Hal \text{ Total}}$	60 %	41 %	30 %	34 %	66 %	74 %
$R_{O_3+NO}/ R_{Hal \text{ Total}}$	32 %	39 %	68 %	60 %	28 %	8.1 %
$R_{O_3+Br}/ R_{Hal \text{ Total}}$	6.2 %	15 %	0.8 %	1.3 %	4.4 %	16 %
$R_{O_3+Cl}/ R_{Hal \text{ Total}}$	0.6 %	0.9 %	0.2 %	0.1 %	0.7 %	0.7 %
$R_{O_3+Br}/ R_{Hal \text{ Total}}^1$	1.6 %	2.4 %	0.2 %	0.3 %	1.4 %	4 %
<i>NoHal</i>						
$R_{O_3+h\nu}/ R_{NoHal \text{ Total}}$	76 %	56 %	71 %	38 %	47 %	78 %
$R_{O_3+NO}/ R_{NoHal \text{ Total}}$	23 %	40 %	27 %	60 %	49 %	21 %
$R_{Hal \text{ Total}}/ R_{NoHal \text{ Total}}^2$	58 %	76 %	81 %	74 %	57 %	38 %

¹Percentages reflect the net effect of R_{O_3+Br} due to null cycles associated with Reactions (R12), (R13) and (R14).

²Relatively lower rates of direct O₃ destruction via all pathways in *Hal* simulations are driven in part by relatively lower steady-state O₃ mixing ratios (see Fig. 7).

with *Hal* were −26 % ($\pm 21\%$) and −27 % ($\pm 12\%$), respectively. Corresponding deviations based on *NoHal* were 42 % ($\pm 25\%$) and 9.3 % ($\pm 15\%$), respectively. For the PBL, although the correlation coefficient for O₃ based on *NoHal* was higher, the *Hal* simulations better reproduce observed O₃ for nearly all stations north of 45° S (Fig. 10). However, simulated PBL O₃ mixing ratios over the high-latitude Southern Hemisphere were substantially underestimated, which indicates that direct and indirect O₃ destruction by Br is overestimated in this region. As mentioned in Sect. 3.1 and discussed in more detail in Sect. 4, available evidence suggests that wind-speed-dependent parameterizations for marine aerosol production such as that used in this study overestimate fluxes of aerosol mass and associated reactive halogens under high-wind conditions. Consequently, though, associated impacts of halogen chemistry on O₃ and other tropospheric species over the high-latitude Southern Ocean are also overestimated. Relative to *Hal*, O₃ at the 500 mb level simulated with *NoHal* was closer to observed O₃ mixing ratios.

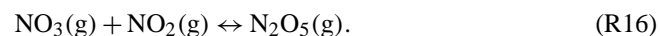
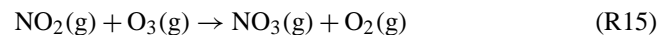
3.4.2 OH : HO₂

Median OH and HO₂ mixing ratios in the PBL simulated with *Hal* were lower by 41 and 18 %, respectively, relative to *NoHal*. Differences were greatest in the MBL and resulted primarily from three processes. First, the enhancement of NO + HO₂ and the addition of BrO + HO₂ → HOBr + O₂ (and subsequent uptake of HOBr by liquid aerosol) are HO₂ sinks. HOBr uptake by aerosols in the MBL was approximately equivalent to OH recycling via HOBr photolysis. Second, the accelerated rate of NO₂ oxidation by halogen species (Sect. 3.3.3), in combination with increased NO in the vicinity of high HO₂ mixing ratios and lower O₃, led to a

net decrease in both OH and HO₂. Third, globally less O₃ reduced the photochemical production of O(¹D). Overall, the OH : HO₂ ratio decreased 28 %, within the range simulated by Keene et al. (2009; 3 to 32 % decrease).

3.4.3 NO_x

The cycling of Cl and Br in the *Hal* simulations impacted distribution, speciation, and lifetimes of NO_x species in two ways. Under polluted conditions at night, N₂O₅ is produced from

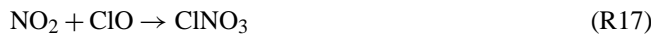


Some N₂O₅ reacts with particulate Cl[−] to produce ClNO₂ via Reaction (R10). In addition, N₂O₅ also hydrolyzes to produce HNO₃, which accounts for 30 % to 50 % of the total NO_x sink in polluted regions (Alexander et al., 2009). The photolysis of ClNO₂ following sunrise via Reaction (R11) regenerates half the NO₂ from which the precursor N₂O₅ was formed and also produces highly reactive Cl atoms. Thus, this pathway (Reactions R15 → R16 → R10 → R11) acts as both a source for halogen radicals and a nocturnal reservoir for NO_x that efficiently extends its atmospheric lifetime, thereby enhancing O₃ production relative to that predicted in the absence of Reactions (R10) and (R11) (as in *NoHal*). Figure 11a depicts the percent deviation of NO_x (NO + NO₂) in the PBL for *Hal* vs. *NoHal* simulations. The increased NO_x lifetime that results primarily from ClNO₂ production and processing is evident in the positive deviations along the primary transport pathways downwind of major pollution sources.

Table 7. WOUDC stations (and corresponding periods of record) at which the vertical profiles in O₃ evaluated herein were measured. Stations are sorted by stop date.

Station code	Station name	Lat	Lon	Altitude (m)	Start date	Stop date
280	Forster	-70.8	11.9	110	May 1985	Feb 1991
21	Edmonton	53.6	-114	766	Jan 1980	Dec 1993
24	Resolute	74.7	-95.0	40	Jan 1980	Dec 1993
67	Boulder	40.0	-105	1634	Jan 1985	Dec 1993
101	Syowa	-69.0	39.6	21	Jan 1986	Dec 1993
26	Aspendale	-38.0	145	1	Jan 1980	Dec 1995
432	Tahiti	-18.0	-149	2	Jan 1998	Dec 1999
175	Nairobi	-1.27	36.9	1795	Jan 1998	Dec 2001
434	San Cristobal	-0.92	-89.6	8	Mar 1998	Dec 2001
435	Paramaribo	5.81	-55.2	25	Oct 1999	Dec 2001
437	Java	-7.57	112	50	Jan 1998	Nov 2002
438	Fiji	-18.1	178	6	Jan 1998	Nov 2002
191	Samoa	-14.3	-170	82	Apr 1986	Dec 2002
219	Natal	-5.84	-35.2	32	Jan 1998	Dec 2002
265	Pretoria	-25.6	28.2	1524	Jul 1990	Dec 2002
436	Reunion	-21.1	55.5	24	Jan 1998	Dec 2002
448	Malindi	-2.99	40.2	-6	Mar 1999	Dec 2002

Under clearer conditions in the MBL, the formation and subsequent hydrolysis of halogen nitrates via



and analogous reactions that produce BrNO₃ accelerate oxidation of NO_x (Sander et al., 1999; Pszenny et al., 2004; Keene et al., 2009). The influence of these reactions is evident in the negative deviations in NO_x simulated by *Hal* relative to *NoHal* for much of the global MBL (Fig. 11a) and in differences in median NO_x mixing ratios simulated with *Hal* vs. *NoHal* for the NH MBL, SH MBL, and PBL. As noted above, the accelerated oxidation of NO_x via these pathways impacts oxidation processes through net O₃ and OH destruction and modified OH/HO₂ ratios. In the Antarctic region, the presence of increased Br, and less O₃ and HO_x increased the lifetime of NO, leading to a positive NO deviation, while NO₂ decreases (Fig. 11b and c).

3.5 Impact of halogens on S cycling

In general, the global-scale sources, lifetimes, and sinks for major S species compare well with the modal-CAM standard chemical scheme and other global model studies of the S budget (8). Major differences between MECCA and modal-CAM are driven in part by influences of halogens in the oxidation of DMS and SO₂, lower OH concentrations in the PBL in MECCA-CAM, and differences in the treatment of H₂SO₄.

The primary DMS oxidation pathways in the conventional mechanism considered in most models are reaction with OH

during daytime and reaction with NO₃ at night. DMS burden and lifetime in *NoHal* are about five times those in the standard modal-CAM, due to lower OH and NO₃ concentrations (factor of two to three for both) in the global PBL. The *Hal* and *NoHal* simulations calculate OH online, while standard modal-CAM uses an offline oxidant database of monthly averages taken from simulations by a chemistry–climate model (Lamarque et al., 2010).

Oxidation of DMS by BrO has been proposed as an important alternate pathway (Toumi, 1994; von Glasow et al., 2002), and oxidation by atomic Cl may also be significant at high Cl-atom concentrations (Keene et al., 1996). Comparison of the major DMS reaction pathways is presented in Table 9. *Hal* simulations indicate that reaction with BrO is important throughout the whole atmosphere, and responsible for 84 % of all DMS oxidation in the Southern Hemisphere MBL. Comparing the total oxidation rate shows that DMS is oxidized faster globally (Table 9, factor of 1.40 in the PBL) than would be predicted by the reaction with OH and NO₃ alone. Globally, median DMS mixing ratios were lower by 74 and 89 % in the PBL and FT, respectively. In contrast, Breider et al. (2010) estimate that oxidation by BrO would decrease DMS mixing ratios in the global MBL by 18 % relative to those predicted based on conventional pathways. The greatest differences in DMS mixing ratios were evident in the SH MBL (Fig. 13c), reflecting faster oxidation in the *Hal* simulations. However, as noted above and discussed in more detail below, production fluxes of reactive halogens and associated impacts on DMS oxidation may be overestimated over the high-latitude Southern Ocean due to overprediction of sea-salt emissions and associated Br activation.

Table 8. Global annual budgets for SO₂, H₂SO₄, nss SO₄²⁻, and DMS, for *Hal* and *NoHal* simulations, and a 5-year simulation using 3-mode modal-CAM (v3.6.33) with its standard chemical module. Ranges of results from previous studies are shown for comparison.

		<i>Hal</i>	<i>NoHal</i>	CAM 3.6.33	Previous studies
SO ₂					
Sources (Tg S y ⁻¹)		79.3	80.6	84.4	83.0–124.6 ^b
Emission		67.5	67.5	67.5	63.7–92.0 ^a
DMS oxidation		11.8	13.1	16.9	10.0–24.7 ^a
Sink (Tg S y ⁻¹)		80.5	82.8	87.0	
Dry deposition		20.3	21.4	22.5	16.0–55.0 ^a
Wet deposition		14.7	13.8	14.6	0.0–19.9 ^a
Gas oxidation		6.2	6.4	11.9	6.1–16.8 ^a
Aqueous oxidation		39.3	41.2	38.0	24.5–57.8 ^a
Burden (Tg S)		0.57	0.57	0.31	0.20–0.61 ^a
Lifetime (d)		2.6	2.6	1.5	0.60–2.6 ^a
H ₂ SO ₄					
Source: SO ₂ + OH		6.2	6.4	11.9	6.1–22.0 ^a
Sink (Tg S y ⁻¹)		5.9	6.2	11.8	
Nucleation		1.2	1.3	0.01	0.05–0.07 ^b
Condensation		4.6	4.8	10.9	13.0–15.2 ^b
Cloud scavenging		0.1	0.1	0.9	
Burden (Tg S)		0.0029	0.0032	1.2 × 10 ⁻³	9.0 × 10 ⁶ –0.001 ^a
Lifetime (h)		4.1	4.4	0.086	0.12–0.17 ^a
Nss SO ₄ ²⁻					
Sources (Tg S y ⁻¹)		46.9	49.1	50.6	59.7 ± 13.2 ^a
Emission		1.7	1.7	1.7	
Aqueous S(IV) oxidation		39.3	41.2	38.0	
Microphysics ^c		5.9	6.2	10.9	
Sink (Tg S y ⁻¹)		45.1	47.3	51.8	
Dry deposition		11.8	12.7	10.3	
Wet deposition		33.3	34.6	41.5	
Burden (Tg S)		0.86	0.88	0.67	0.66 ± 0.17 ^a
Lifetime (h)		5.6	5.4	4.8	4.1 ± 0.74 ^a
DMS					
Sources: emission (Tg S y ⁻¹)		18.3	18.3	18.3	10.7–23.7 ^a
Sinks: gas oxidation (Tg S y ⁻¹)		18.3	18.3	18.4	
Burden (Tg S)		0.032	0.15	0.029	0.02–0.15 ^a
Lifetime (h)		0.64	3.0	0.57	0.024–0.13 ^a

^aFrom Liu et al. (2012) and references therein. ^bFrom Spracklen et al. (2005) and references therein. ^cCombined source of nss SO₄²⁻ due to H₂SO₄(g) nucleation, condensation, and scavenging.

As for most other multiphase 3-D models, limitations in the capabilities of current high-performance platforms effectively preclude explicit evaluation of the chemical evolution of freshly produced particles as a function of age. Aerosols of each size fraction emitted during each time step are mixed with preexisting aerosols in that size fraction, and the bulk composition is adjusted accordingly. Freshly produced marine aerosol are alkaline, but, in most marine regions, acids and acid precursors (SO₂, HNO₃, HCl, HCOOH, and CH₃COOH) are present at levels sufficient to titrate

marine-derived alkalinity associated with all but the largest aerosols within tens of minutes after emission (e.g., Erickson et al., 1999). Consequently, in most marine regions, most aerosols in ambient air are acidic (e.g., Erickson et al., 1999; Keene et al., 2009). As a result, when fresh alkaline aerosols are mixed with preexisting acidic aerosols in the model, the fresh alkalinity is immediately titrated and, thus, chemical processes that are limited to alkaline conditions are not resolved. In alkaline aerosol solutions, oxidation of S(IV) by O₃ is the dominant source for nss SO₄²⁻; rates are diffusion

Table 9. Relative contributions of different reaction pathways (R) to total DMS and S(IV) oxidation in *Hal* and in *NoHal* simulations, and the corresponding total DMS and S(IV) oxidation via all pathways in *Hal* vs. *NoHal* simulations expressed as percentages; based on ANN means, and spatial medians for different regions of the atmosphere. Subscripts aq and cl designate aerosol and cloud-water reactions, respectively.

	PBL	FT	Troposphere	NH CBL	SH CBL	NH MBL	SH MBL
DMS(<i>Hal</i>)							
$R_{\text{DMS}+\text{OH}} / R_{\text{DMS-Hal-Total}}$	6.6 %	27 %	8.3 %	9.3 %	18 %	12 %	4.0 %
$R_{\text{DMS}+\text{NO}_3} / R_{\text{DMS-Hal-Total}}$	11 %	14 %	11 %	69 %	53 %	24 %	3.8 %
$R_{\text{DMS}+\text{Cl}} / R_{\text{DMS-Hal-Total}}$	14 %	8.4 %	14 %	9.3 %	5.0 %	20 %	9.1 %
$R_{\text{DMS}+\text{BrO}} / R_{\text{DMS-Hal-Total}}$	68 %	50 %	67 %	12 %	24 %	44 %	82 %
DMS(<i>NoHal</i>)							
$R_{\text{DMS}+\text{OH}} / R_{\text{DMS-NoHal-Total}}$	54 %	74 %	57 %	13 %	31 %	34 %	66 %
$R_{\text{DMS}+\text{NO}_3} / R_{\text{DMS-NoHal-Total}}$	46 %	26 %	43 %	87 %	69 %	66 %	34 %
$R_{\text{DMS-Hal-Total}} / R_{\text{DMS-NoHal-Total}}^*$	140 %	52 %	122 %	73 %	43 %	118 %	227 %
S(IV)(<i>Hal</i>)							
$R_{\text{SO}_2+\text{OH}} / R_{\text{S(IV)-Total}}$	11 %	13 %	11 %	11 %	5.7 %	18 %	6.5 %
$R_{\text{S(IV)aq}+\text{H}_2\text{O}_2} / R_{\text{S(IV)-Hal-Total}}$	1.3 %	0.6 %	1.2 %	1.0 %	0.2 %	2.3 %	2.0 %
$R_{\text{S(IV)aq}+\text{O}_3} / R_{\text{S(IV)-Hal-Total}}$	0.1 %	0.0 %	0.1 %	0.0 %	0.1 %	0.0 %	0.8 %
$R_{\text{S(IV)aq}+\text{HOCl}} / R_{\text{S(IV)-Hal-Total}}$	0.9 %	0.2 %	0.8 %	0.1 %	0.0 %	2.0 %	4.9 %
$R_{\text{S(IV)aq}+\text{HOBr}} / R_{\text{S(IV)-Hal-Total}}$	0.2 %	0.1 %	0.2 %	0.0 %	0.0 %	0.0 %	2.0 %
$R_{\text{S(IV)cl}+\text{H}_2\text{O}_2} / R_{\text{S(IV)-Hal-Total}}$	74 %	81 %	75 %	60 %	90 %	73 %	81 %
$R_{\text{S(IV)cl}+\text{O}_3} / R_{\text{S(IV)-Hal-Total}}$	12 %	1.9 %	11 %	27 %	4.2 %	4.8 %	2.1 %
$R_{\text{S(IV)cl}+\text{HOCl}} / R_{\text{S(IV)-Hal-Total}}$	0.2 %	1.3 %	0.4 %	0.1 %	0.0 %	0.0 %	0.2 %
$R_{\text{S(IV)cl}+\text{HOBr}} / R_{\text{S(IV)-Hal-Total}}$	0.6 %	1.8 %	0.8 %	0.8 %	0.2 %	0.2 %	0.5 %
$R_{\text{S(IV)aq}} / R_{\text{S(IV)cl}}$	2.8 %	1.1 %	2.6 %	1.4 %	0.3 %	5.6 %	12 %
S(IV)(<i>NoHal</i>)							
$R_{\text{SO}_2+\text{OH}} / R_{\text{S(IV)-NoHal-Total}}$	10 %	14 %	11 %	8.5 %	5.0 %	17 %	9.1 %
$R_{\text{S(IV)aq}+\text{H}_2\text{O}_2} / R_{\text{S(IV)-NoHal-Total}}$	1.1 %	0.5 %	1.0 %	0.8 %	0.1 %	1.5 %	1.9 %
$R_{\text{S(IV)aq}+\text{O}_3} / R_{\text{S(IV)-NoHal-Total}}$	0.2 %	0.0 %	0.2 %	0.0 %	0.0 %	0.0 %	3.1 %
$R_{\text{S(IV)cl}+\text{H}_2\text{O}_2} / R_{\text{S(IV)-NoHal-Total}}$	76 %	81 %	76 %	59 %	90 %	74 %	83 %
$R_{\text{S(IV)cl}+\text{O}_3} / R_{\text{S(IV)-NoHal-Total}}$	13 %	5.1 %	12 %	31 %	5.3 %	7.5 %	2.8 %
$R_{\text{S(IV)aq}} / R_{\text{S(IV)cl}}$	1.5 %	0.6 %	1.4 %	0.9 %	0.1 %	1.9 %	5.9 %
$R_{\text{S(IV)-Hal-Total}} / R_{\text{S(IV)-NoHal-Total}}^*$	88 %	88 %	89 %	88 %	87 %	86 %	89 %

*Differences are driven in part by corresponding differences in steady-state concentrations of DMS and S(IV) in *Hal* and *NoHal* simulation.

limited (Chameides and Stelson, 1992; Keene et al., 1998). SO_2 solubility and its associated aqueous-phase oxidation by O_3 decrease with increasing acidity, and, consequently, this pathway becomes unimportant after the initial alkalinity has been titrated and pH drops (Chameides and Stelson, 1992; Keene et al., 1998). In most regions, the rapid acidification of fresh aerosol limits nss SO_4^{2-} production from S(IV) oxidation by O_3 (Erickson et al., 1999). However, in more remote regions where continental sources of acids are relatively less important and high wind velocities over long fetch sustain high fluxes of marine aerosols and associated alkalinity, such as the MBL over the high-latitude Southern Ocean, the O_3 pathway may be relatively more important. Because our model structure does explicitly resolve S(IV) oxidation in freshly produced marine aerosol, simulated rates of SO_2

oxidation and nss SO_4^{2-} production reported herein are considered lower limits.

The SO_2 budgets for the *Hal* and *NoHal* simulations are similar. In comparison to the standard modal-CAM, the main difference is the lower gas-phase oxidation due to lower PBL OH concentration in MECCA-CAM, and slower aqueous uptake. In both *Hal* and *NoHal* simulations, oxidation by H_2O_2 in the cloud water aqueous phase was the single most important sink for SO_2 globally (Table 9). In the *Hal* simulation, oxidation of S(IV) in deliquesced aerosols accounted for about 12 % of S(IV) oxidation in the SH MBL, but only 1 % globally. As noted above, aqueous-phase pathways for S(IV) oxidation in aerosol solutions are strongly pH dependent (Chameides and Stelson, 1992; Keene et al., 1998). For size fractions that overlap, simulated aerosol pHs based on *Hal* are reasonably representative of available estimates

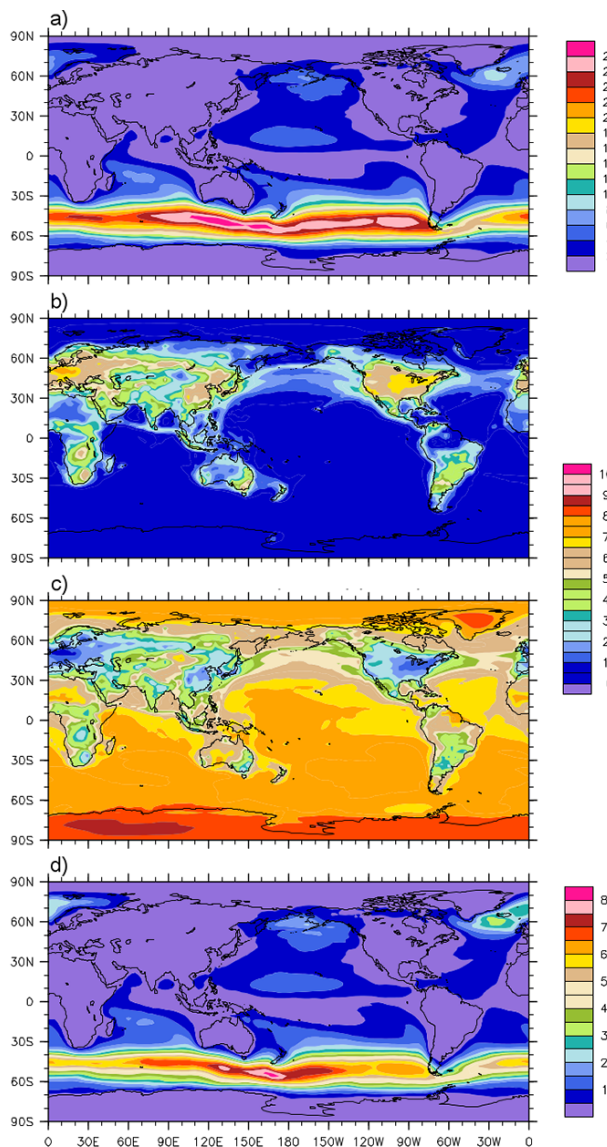


Fig. 8. (a) Percent contribution of Reaction (R1) to total O₃ destruction in PBL (see Table 6). (b) Ratio of Reactions (R12) to (R1), in percent. (c) Ratio of Reaction (R13) to (R1). (d) Percent contribution of Reaction (R1) less the sum of Reactions (R12), (R13) and (R14) to total O₃ destruction in the PBL. Due to its small contribution to the null cycle, Reaction (R14) is not shown.

inferred from direct measurements (Fig. 3). The higher pHs sustained by acid displacement in the *Hal* vs. *NoHal* simulation resulted in a much greater uptake of SO₂ in aerosol (Fig. 13b). SO₂(g) and aerosol S(IV) simulated for the ANN PBL by *Hal* vs. *NoHal* (Fig. 13a, b) diverged by median values of -7.73% (-77.4 to 686%) and 428% (-99.9 to $1.87 \times 10^7\%$), respectively. These differences are driven primarily by the lower aerosol solution pHs (by 1 to 2 units) in *NoHal*. Significant aqueous-phase oxidation of S(IV) by O₃ in aerosol solutions is limited to alkaline conditions

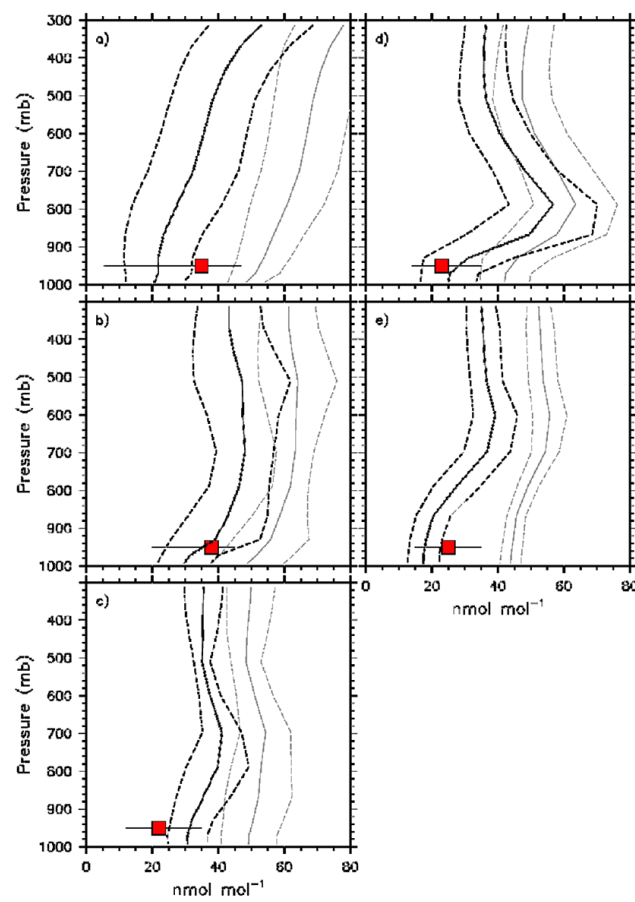


Fig. 9. Vertical profiles of mean O₃ (nmol mol⁻¹; solid) and standard deviation (dashed) simulated with *Hal* (black) and *NoHal* (gray) and the corresponding mean O₃ measured in near-surface air (red boxes) for the (a) EURO, (b) NAFR, (c) ITCZ, and (d) SATL regimes as reported by Keene et al. (2009) and at (e) Hawaii (Pszenny et al., 2004). Bars depict measurement ranges.

(Chameides and Stelson, 1992), and, consequently, this pathway was important only in the SH where persistent high winds sustain high concentrations of marine aerosol (Long et al., 2011), sources of acidity are relatively low, and, thus, pH values are relatively high (see Tables S1 and S2). The lower pH of aerosol solutions in other regions efficiently suppressed aerosol S(IV) oxidation by O₃ in *Hal* simulations (Table 9). Aqueous-phase oxidation of S(IV) by HOCl and HOBr enhances production of S(VI) in moderate acidity (pH 5 to 6 aerosol; Vogt et al., 1996; Keene et al., 1998; von Glasow et al., 2002), but production via these pathways decreases with decreasing pH due to the lower solubility of SO₂ (Keene et al., 2009). In most regions, the pH range of 5 to 6 is transient and acidified aerosols rapidly equilibrate with atmospheric acids at somewhat lower pHs. Consequently, *Hal* simulations indicate that oxidation of S(IV) by hypohalous acids accounts for minor to negligible fractions of S(IV) oxidation in the MBL globally (Table 9). Differences in our

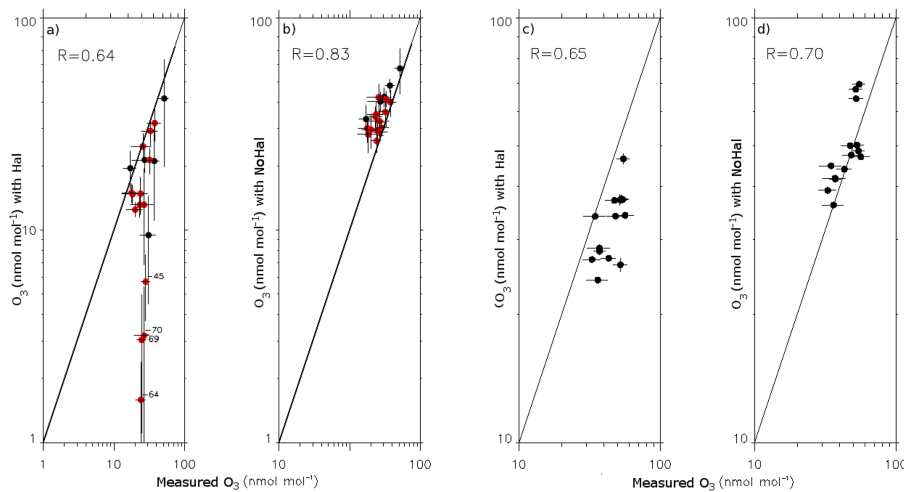


Fig. 10. O_3 simulated in the PBL with (a) *Hal* and (b) *NoHal*, and at the 500 mb pressure height for (c) *Hal* and (d) *NoHal* vs. the WOUDC O_3 climatology. Horizontal and vertical bars represent measurement and simulated standard deviations, respectively. The corresponding correlation coefficients (R) are shown. In (a) and (b), red symbols represent stations at or south of the Equator. In (a), approximate latitudes of stations with four highest modeled O_3 underpredictions are indicated.

results compared to von Glasow et al. (2002) were due to the inability to differentiate between cloudy and non-cloudy conditions in our monthly-mean model data sets, whereas von Glasow et al. (2002) were able to explicitly differentiate processes under clear-sky and cloudy conditions.

The most noticeable budget differences between CAM/MECCA and the standard modal-CAM are for H_2SO_4 vapor. In *Hal* and *NoHal*, the H_2SO_4 source (from SO_2 reaction with OH) is smaller, but the burden and lifetime are higher, which was driven by several factors. First, the lower PBL OH concentrations in *Hal* and *NoHal* result in more SO_2 being mixed into the FT where the total aerosol surface area and liquid water content are low and $H_2SO_4(g)$ loss by condensation is relatively slow, resulting in higher burdens and lifetimes. Modal-CAM calculates H_2SO_4 vapor production (by gas-phase chemistry) and uptake by aerosols sequentially, while *Hal* and *NoHal* calculate them simultaneously, which has been shown to affect H_2SO_4 vapor concentrations (Kokkola et al., 2009). In addition, modal-CAM uses the Fuchs–Sutugin equation to calculate H_2SO_4 mass-transfer rates from gas to particle phases, whereas *Hal* and *NoHal* use the method of Schwartz (1986), yielding mass-transfer rates generally slower in *Hal* and *NoHal* relative to modal-CAM (Sander, 1999). A more detailed evaluation of differences in the simulated H_2SO_4 vapor concentrations is beyond the scope of this study. The higher $H_2SO_4(g)$ concentrations in the FT also lead to higher rates of nucleation and growth of new particles in *Hal* and *NoHal*. Particle number concentrations based on enhanced nucleation in *Hal* yielded reasonably good agreement with observations from a wide range of locations (Table 11), while other studies report underestimations of concentrations under similar conditions (Adams and Seinfeld, 2002;

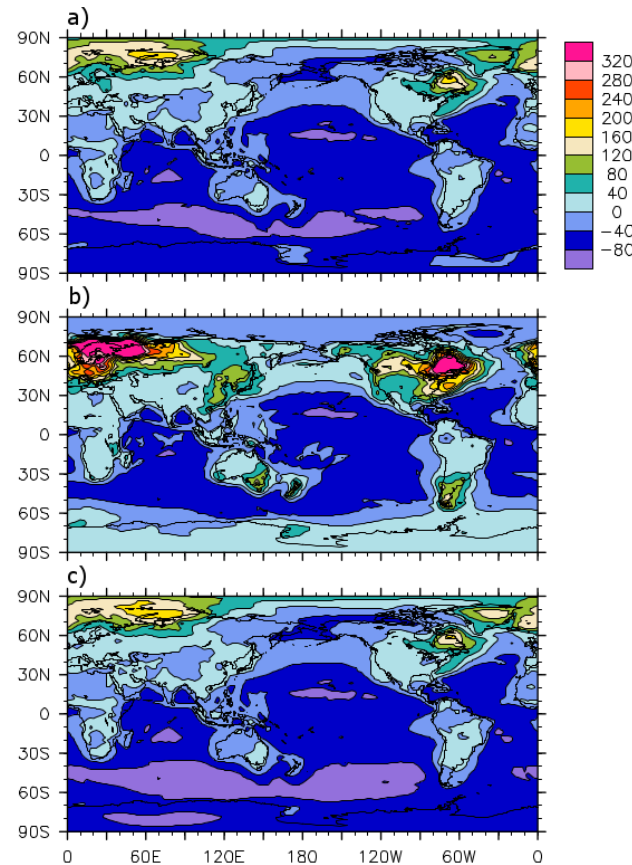


Fig. 11. Percent deviation of (a) NO_x ($NO + NO_2$), (b) NO , and (c) NO_2 in the PBL for *Hal* vs. *NoHal* simulations.

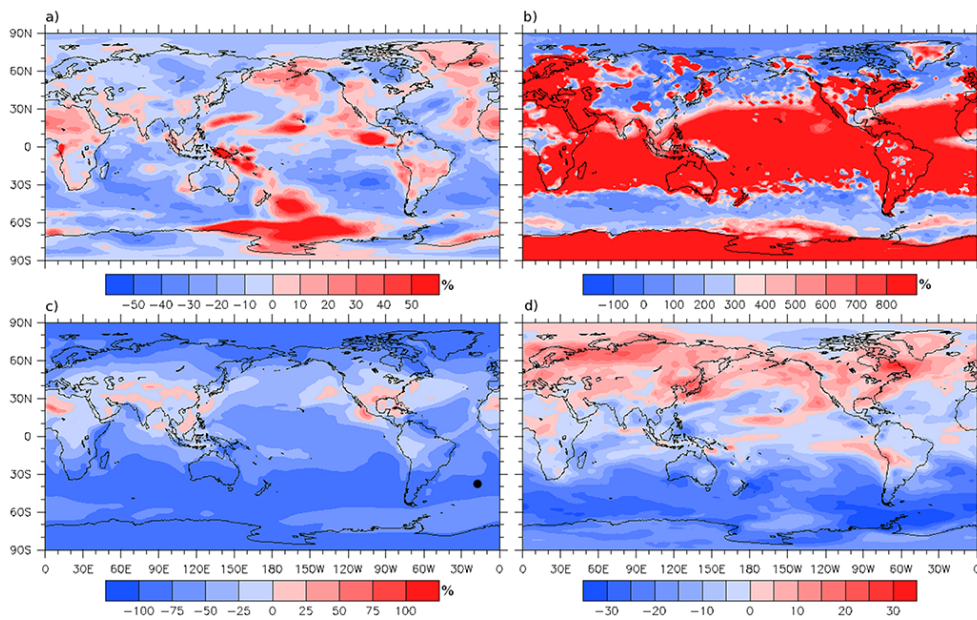


Fig. 12. Percent deviations in ANN PBL *Hal* vs. *NoHal* for (a) SO_2 , (b) aggregate aqueous S(IV) ($\text{SO}_{2(\text{aq})}$, HSO_3^- , and SO_3^{2-} summed over the three simulated size bins), (c) DMS and (d) aggregate nss SO_4^{2-} .

Spracklen et al., 2005). These differences are important to aerosol microphysics in the FT, and thus deserve further investigation. However, they do not significantly impact the budget or distribution of nss SO_4^{2-} in our simulations.

The global nss SO_4^{2-} budgets for *Hal* and *NoHal* were nearly indistinguishable, while, compared to a 5-year simulation of the standard modal-CAM, the nss SO_4^{2-} burden and lifetimes were 30 to 40 % higher (Table 8). Globally, nss SO_4^{2-} shifted to smaller size bins driven by transport and subsequent oxidation of SO_2 from the PBL into the FT in the CAM-MECCA system vs. standard modal-CAM. While the global S budgets for *Hal* and *NoHal* are similar, concentrations of nss SO_4^{2-} in the PBL vary regionally by $\pm 30\%$. In the NH PBL, nss SO_4^{2-} was generally higher in *Hal* (Fig. 12d) due to enhanced gas-phase and aqueous-aerosol oxidation of SO_2 (Fig. 12b), less oxidation in cloud droplets, and the shorter lifetime of nss SO_4^{2-} produced in cloud droplets. Lower nss SO_4^{2-} in *Hal* for the Indian and southeast Asian PBL was driven in part by an $\sim 10\%$ increase in rain and wet removal. A detailed evaluation of interactions between chemistry, weather and climate is beyond the scope of this paper. The largest relative (Fig. 12d) and absolute (not shown) nss SO_4^{2-} positive deviations occurred immediately downwind of large anthropogenic sources of SO_2 in eastern China and the eastern USA. This was due to higher aerosol pH leading to more SO_2 uptake (Fig. 12a and b). Directly further upwind from these nss SO_4^{2-} deviation maxima, aqueous S(IV) deviations become negative, resulting from enhanced oxidation of S(IV) by aqueous halogen radicals (HOCl and HOBr). In addition, a significant positive

global correlation between nss SO_4^{2-} and aerosol liquid water ($R^2 = 0.55$; $p < 0.01$) in the PBL suggests a non-linear positive feedback link between aerosol hygroscopicity and its ability to take up and oxidize SO_2 in the aqueous phase. In the SH, the nss SO_4^{2-} burden decreased by 19 % on average, due to faster gas-phase oxidation of DMS (primarily by BrO) and somewhat lower yield of SO_2 , more efficient uptake of SO_2 in larger aerosol particles with higher pH, and faster deposition of the nss SO_4^{2-} formed in the larger particles (see Tables 7 and 8). Based on comparisons with observations, *Hal* and *NoHal* provided similar resolution in predicting mean annual SO_2 and nss SO_4^{2-} (Fig. 13, Table 11).

Relative to the conventional pathways considered in *NoHal* and most other models, the net global effects of halogen chemistry on S cycling in marine air are accelerated oxidation of DMS thereby reducing its atmospheric lifetime. Despite relatively large influences on some pathways in the marine S cycle (Table 8), the domination of S cycling by continental and anthropogenically influenced air masses (where halogen chemistry is relatively less important) and by non-halogen aqueous chemistry in clouds limited the overall net effect of halogens on the atmospheric S budget. However, simulated results suggest potential non-linear feedbacks that may significantly alter nss SO_4^{2-} distributions downwind of major sources.

3.6 NMHCs and CH_4

The oxidation of CH_4 and NMHCs is one of the primary sources of O_3 in the troposphere through the production of organic peroxy radicals that short-circuit the destruction of

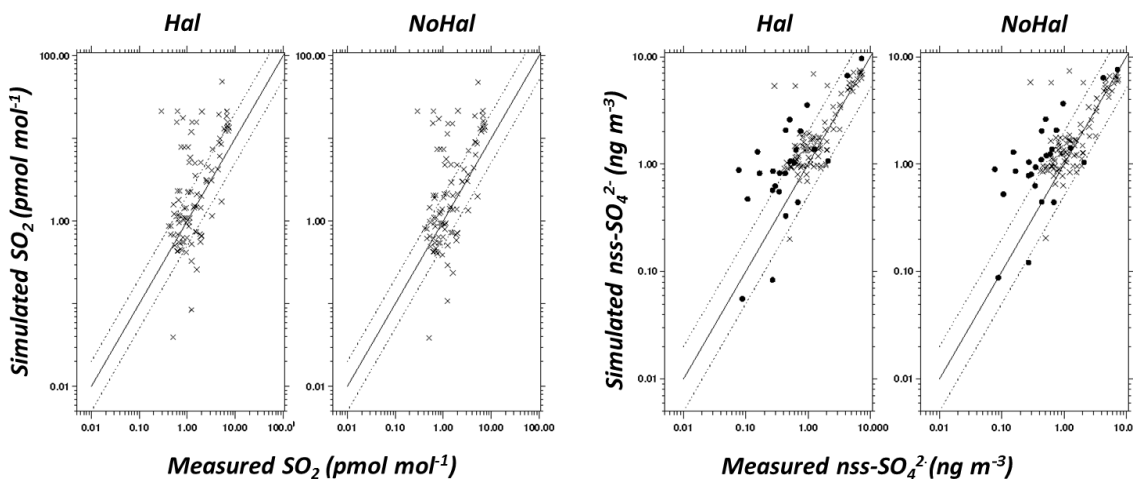


Fig. 13. Mean SO₂ measured by the IMPROVE network at continental sites in the US vs. mean SO₂ in the surface layer of the corresponding grid cell simulated with (a) *Hal* and (b) *NoHal*. Mean nss SO₄²⁻ measured at continental sites by the IMPROVE network (designated by x's) and at marine sites by Atmosphere–Ocean Chemistry Experiment (AEROCE; Savoie et al., 2002), US Department of Energy as the Environmental Measurements Laboratory (DOE-EML), and the Sea–Air Exchange Experiment (SEAREX; Riley et al., 1989) (designated by dark circles) vs. mean nss SO₄²⁻ in the surface layer of the corresponding grid cells simulated with (c) *Hal* and (d) *NoHal*.

O₃ by NO. Relative to the *NoHal*, reactions involving halogens in *Hal* decreased the total rate of CH₃O₂ formation by 9 and 13 % in the PBL and FT, respectively, and total CH₃O₂ destruction by 2 and 14 % in the PBL and FT, respectively. These reactions resulted in lower steady-state mixing ratios of CH₃O₂ throughout most of the global troposphere (not shown). CH₃O₂ in the FT did not vary significantly between the two runs.

Averaged globally, in combination with lower OH plus reaction with atomic Cl, CH₄ oxidation rates decreased by 3 % relative to the *NoHal* simulation. The corresponding oxidation rates in the continental and marine boundary layer were higher by 13 and 9 %, respectively, reflecting the production of atomic Cl in the lower atmosphere. While atomic Cl mixing ratios were comparable to (sparse) inferred observations, simulated CH₄ mixing ratios were fixed throughout the atmosphere. As such, these results are considered upper limits.

4 Discussion

Results reported herein provide useful insight regarding the potential importance of halogen cycling in tropospheric chemistry and physics, limitations in our current understanding of the associated chemical pathways as implemented in the MECCA chemical mechanism, and the sensitivity of halogen chemistry to atmospheric physics and circulation. Comparisons with observations indicate that wind-speed-dependent parameterization schemes for marine aerosol used in this and other global models overestimate marine aerosol production over the high-latitude Southern Ocean. Comparisons indicate further that the full MECCA chemical mechanism overestimates rates of Br activation and radical pro-

duction and recycling consistent with previous reports (e.g., Keene et al., 2009; Sommariva and von Glasow, 2012). Finally, our model does not consider processes involving iodine species and their associated interactions in Br and Cl cycling (e.g., Read et al., 2008; Saiz-Lopez et al., 2012). The net effect is that results reported herein overestimate the overall impact of Br chemistry globally, and thus caution is warranted in their interpretation and extrapolation to the ambient environment. However, with the exception of adjusting total stratospheric O₃ to climatological values, MECCA was implemented without any prescribed adjustments intended to “tune” simulated results to observations. Consequently, deviations between simulations and observations can be interpreted directly in terms of gaps in our understanding of the underlying processes. Results also provide useful qualitative insight regarding details of halogen cycling.

Comparisons between simulated conditions and measurements indicate that the coupled MECCA/modal-CAM mechanism reproduces important characteristics of the multiphase chemical composition of the troposphere including aerosol pH, Cl chemistry in continental and coastal air, and Cl and Br species in some regions of the global MBL. Some of these characteristic have not been previously simulated explicitly at the global scale. In addition, the simulation of EF(Br) within the range of observations coupled with the model’s dependence upon interactions between the FT and PBL in the enrichment process suggests that (1) the cycling of sea-salt-derived Br is important in the FT; (2) that FT Br cycling is tightly coupled with PBL chemistry; (3) global-scale circulation and dynamics play a large role in the global distribution, partitioning, and impacts of inorganic Br species; and (4) release and cycling of Br from marine aerosol is highly

Table 10. Mean particle number concentrations \pm standard deviations when available (cm^{-3}) measured at surface locations and the median, range, \log_{10} -normal mean and relative standard deviation for number concentrations simulated with *Hal* in the surface layer of the corresponding grid cells. Simulated values are summed across all three particle modes.

Location	Observed	Simulated (<i>Hal</i>)				Source
		Median	Max	Min	Mean ($\pm 10^\sigma$)	
Alkmaar, Netherlands	$25\ 800 \pm 11\ 300$	2597	23508	815	$2814 \pm 10^{9.4}\%$	Ruuskanen et al. (2001)
Erfurt, Germany	$25\ 900 \pm 12\ 200$	2767	35180	759	$2977 \pm 10^{11.8}\%$	Ruuskanen et al. (2001)
Helsinki, Finland	$20\ 300 \pm 8200$	2628	13134	610	$2839 \pm 10^{11.0}\%$	Ruuskanen et al. (2001)
Pittsburg, PA, USA	16470	13037	48678	2592	$12\ 566 \pm 10^{8.0}\%$	Stanier et al. (2004)
Beijing, PRC	$29\ 000 \pm 10\ 000$	11340	66393	1697	$11\ 082 \pm 10^{7.5}\%$	Leitte et al. (2011)
Indian Ocean (north of ITCZ)	856 \pm 232	324	1393	151	$387 \pm 10^{7.9}\%$	Kamra (2003)
Indian Ocean (ITCZ)	418 \pm 151	232	1277	74	$248 \pm 10^{7.1}\%$	Kamra (2003)
Indian Ocean (south of ITCZ)	334 \pm 20	277	884	104	$309 \pm 10^{6.8}\%$	Kamra (2003)
Melpitz, Germany	4830	2767	35180	759	$2977 \pm 10^{11.8}\%$	Birmili et al. (2001) ^a
Hyttiälä, Finland	1813 ± 1525	1708	7846	415	$1693 \pm 10^{10.7}\%$	Mäkelä et al. (2000)

^aAs reported by Spracklen et al. (2005).

Table 11. Correlation coefficients (*R*), normalized mean square error (NMSE), and mean deviations of measured $\text{SO}_2(\text{g})$ and nss SO_4^{2-} vs. mean simulated values in the surface layer of the corresponding grid cell with *Hal* and *NoHal*, as plotted in Fig. 13. Continental measurement are from the IMPROVE network; marine measurements are from the Atmosphere–Ocean Chemistry Experiment (AEROCE; Savoie et al., 2002), US Department of Energy as the Environmental Measurements Laboratory (DOE-EML), and the Sea–Air Exchange Experiment (SEAREX; Riley et al., 1989).

		<i>R</i>	NMSE	Mean deviation
<i>Hal</i>	$\text{SO}_2(\text{g})$	0.53	2.9	$2.7 (\pm 8.8)$
	Continental nss SO_4^{2-}	0.87	0.083	$0.59 (\pm 2.0)$
	Marine nss SO_4^{2-}	0.93	0.083	$1.9 (\pm 2.6)$
<i>NoHal</i>	$\text{SO}_2(\text{g})$	0.54	2.8	$2.6 (\pm 8.8)$
	Continental nss SO_4^{2-}	0.82	0.095	$0.55 (\pm 2.2)$
	Marine nss SO_4^{2-}	0.89	0.086	$2.1 (\pm 2.6)$

sensitive to the marine aerosol flux. The results also suggest that SO_2 oxidation by HOBr and HOCl primarily in the FT plays a central role in this dynamic connection.

Additional research is needed to resolve outstanding uncertainties in the fully coupled physicochemical system and thereby facilitate more representative model studies. For example, comparison of simulated and observed Br_t reveals a fairly consistent pattern of model overprediction. With the exception of the southeastern North Atlantic MBL adjacent to northern Africa, where the agreement was good, the model overpredicted Br_t by factors of 2 to 6 (Table 3). Adding Br produced in association with organic Br-containing species to the simulation (which may account for 27 % of the global Br_t source; Parrella et al., 2012) would exacerbate these differences. In this regard, we note that, with the exception of

Hawaii, the geographic locations in Table 3 were coincident with large gradients in NO_x and Br_t . The coarse model resolution relative to such gradients in these regions constrains the reliability of such direct comparisons between observed and simulated values and probably contributes to divergence in these results. Simulated and measured BrO at open-ocean locations are much closer in value (Table 4).

Principal component analysis of reaction rates in this study suggests that overproduction of BrCl via Reactions (R5), (R6), and (R7) may account for overestimates in Br activation and recycling. Box model calculations based on the MECCA scheme indicate that this reaction pathway drives large fractions of aerosol debromination over a wide range in chemical regimes (Keene et al., 2009). Sommariva and von Glasow (2012) also report overproduction of BrCl in the simulated tropical marine boundary layer. In contrast, measurements of BrCl at Cape Verde were all below detection limits ($< 2 \text{ pmol mol}^{-1}$) (Lawler et al., 2009). Further, for all regimes simulated by Keene et al. (2009), BrCl alone can account for virtually all of the difference between modeled and observed Br_t . Like Sommariva and von Glasow (2012), we conclude that some as yet unresolved mechanism is acting to limit aerosol debromination via Reaction (R6). It seems less likely that the rate of Reaction (R6) is incorrect; rather some potential bromide-yielding reaction with HOBr or BrCl may be missing. Alternatively, uptake of HOBr and degassing of BrCl may be limited in a way unaccounted for in our model. In this regard, we note that the Henry's law constant and accommodation coefficients for BrCl are estimated. More generally, published values of Henry's law constants (K_H) of several species governing gas–aerosol partitioning vary by large amounts. For example, published K_H values for Br_2 , BrCl and HBr differ by factors of two or more, and those for HCl differ by three orders of magnitude (see <http://www.henrys-law.org> for a detailed compilation of

Henry's law constants). Organic surface layers on marine aerosol may also alter rates of gas-phase transfer processes (e.g., Kolb et al., 2010). Sommariva and von Glasow (2012) hypothesize that dissolved organic matter in aerosol solutions may react with Br and Cl radicals, yielding halide ions and thereby slowing production of BrCl and Br₂. Both fresh and ambient marine aerosol are known to be highly enriched in organic matter (Long et al., 2011, and references therein). The above points to the need for experiments to evaluate the potential role of organic matter in inorganic halogen cycling.

Lastly, in contrast to the relatively good agreement between simulated and measured O₃ in other regions, comparisons in the SH MBL below 45° S indicate that the model systematically underpredicts O₃ concentrations by up to 93 % (Figs. 7 and 10). As noted above, comparisons between simulated aerosol loadings and AOD over the high-latitude Southern Ocean (Jaegle et al., 2011) suggest that simulated aerosol production based on wind-speed-dependent parameterizations such as that used for this study (Long et al., 2011) and the associated impacts of halogen chemistry in this region may be too high. In addition, simulated concentrations of marine aerosol south of 45° S are greater by factors of 2 to 13 relative to measured concentrations (Prospero et al., 1989; Savoie et al., 1989, 1993; Arimoto et al., 1996). Between 45° S and 80° S, modeled Br_t, Br, and Br₂ correlated strongly with sea-salt mass (R^2 of 0.49, 0.77 and 0.42, respectively), which is consistent with the fact that Br is controlled primarily by Br₂ emission from marine aerosol, its subsequent photolysis, and the cycling to Br via BrO self-reaction (Table 5). Median BrCl simulated in the SH MBL is a factor of four to five less than that in the NH MBL and a factor of eight less than that modeled in the South Atlantic by Keene et al. (2009) (see Supplement). The simulated median for the SH MBL is below current instrumental detection limits (e.g., $\sim 2.0 \text{ pmol mol}^{-1}$; Lawler et al., 2009). The lack of comprehensive observations of Br speciation in the SH MBL precludes analysis. Based on the above, we infer that the primary cause for the overpredicted loss of O₃ due to halogen reactions in this region is an overestimate of marine aerosol production and the associated activation of Br₂.

Despite these limitations, our results indicate that, qualitatively, reactions involving sea-salt-derived halogens destroyed O₃ throughout the MBL and the global troposphere both directly via reaction with halogen radicals and indirectly via the accelerated oxidation of NO_x through the formation and processing of halogen nitrates. The role of null cycles associated with Reactions (R12) and (R13) cannot be neglected in mechanisms and analysis considering interactions between Br and O₃. To this end, we note that Reaction (R12) is not included in the Br mechanism used in Parrella et al. (2012), which constrains interpretation of the impacts of Br over land and in proximity to NO_x sources. *Hal* simulations also indicate that the formation and processing of CINO₂ in the polluted NH PBL increase the atmospheric lifetime and transport of NO_x, alter NO–NO₂ partitioning,

and activate significant atomic Cl with associated implication for oxidation processes. NSS-SO₄²⁻ lifetimes were extended immediately downwind of major sources of SO₂ due to the enhanced uptake of SO₂ by higher-pH aerosol in the *Hal* simulation vs. *NoHal*. The oxidation of DMS and to a lesser extent S(IV) by halogens in the MBL modified regional S cycling relative to that based on conventional chemical pathways considered in most models. DMS oxidation was enhanced by the reaction with BrO and Cl, accounting for 60 % of DMS oxidation throughout the model troposphere. In the *Hal* simulation, reactions in aqueous aerosol particles accounted for 12 % of the total S(IV) oxidation in the SH MBL, but only about 1 % globally. Reaction with HOCl and HOBr in moderately acidic aerosol solutions increased S(IV) oxidation rates in the PBL by only 1.2 %. As with O₃, it is likely that the estimates of DMS and S(IV) oxidation in the high southern latitudes is overestimated due primarily to an overestimation of sea-salt emission, and subsequent activation of associated halogens. A decrease in sea-salt emission of 40 %, per estimates by Jaegle et al. (2011), yielding a proportional decrease in available reactive Br and Cl, would reduce this impact by approximately a factor of two. Overall, halogen chemistry increased rates of S(VI) production from precursors.

Although a detailed evaluation of halogen cycling on radiation, precipitation, and related climate processes was beyond the scope of this analysis, results presented here have important implications for feedbacks between the atmospheric chemistry, anthropogenically forced changes in atmospheric composition, and Earth's climate system. The continued expansion of the human population and global-scale industrialization will result in increased emissions of acids and acid precursors. Halogen activation and radical recycling are acid catalyzed (Keene et al., 1998); and increased acidification of marine aerosol in remote regions such as the high-latitude Southern Hemisphere would lead to increased activation of halogen species with associated implications for tropospheric evolution. It has been hypothesized that modest increases in acidity in this region would yield disproportionately large increases in Cl and Br activation rates (Sander et al., 2003). This study suggests that large-scale changes in halogen activation in the MBL would impact the deeper troposphere. However, the long-term implications of increased activation cannot be evaluated explicitly based on short-term simulation studies such as those reported herein.

In addition, current projections indicate that climate change will alter global and regional wind fields. Since marine aerosol production scales exponentially with wind speed, such changes would have major consequences for the production, atmospheric concentrations, and processing of marine aerosol. Although the potential climatic implications of changes in marine aerosol production cannot be assessed directly based on this study, our results suggest that they would be important. Available evidence indicates that greater sea-salt emissions will result in greater Br activation

and associated radical chemistry and influences on tropospheric composition (Sander et al., 2003; Keene et al., 2009).

Lastly, inorganic Br is believed to be a primary Hg oxidant in the atmosphere and may control Hg's atmospheric lifetime and deposition (Holmes et al., 2010). Large-scale emission of Hg to the atmosphere in South America associated with artisanal gold mining, combined with the potential for accelerated activation of reactive Br into the Southern Hemisphere due to industrialization, could pose a significant regional- to global-scale hazard.

Future research to address these issues would require the capacity to run century-scale simulations using a fully coupled (with an ocean model) configuration. To this end, the computational limitations of the system used here are prohibitively large. Additional effort is needed to increase the efficiency of the chemical solution and improve the capacity to store data.

Despite the limitations discussed above, estimated impacts of sea-salt-derived Cl and Br on HO_x, NO_x, O₃, and S in the NH and the tropical SH provide useful context for understanding halogen cycling and identifying important uncertainties. Other features of the simulations point to potentially important processes that should be considered in the context of interpreting observations. For example:

1. The model's prediction of observed phenomena like BrO maxima in the Antarctic free troposphere, the presence of sea-salt-derived Br over the Arctic during spring, and Br enrichments of PBL aerosols suggest that large-scale dynamics plays an important role in halogen cycling.
2. The large influence of halogen chemistry in the SH MBL, while overestimated, highlights large uncertainties in current understanding of marine aerosol and, more generally, air-sea exchange processes at energetic sea states and the need for new research to resolve discrepancies.
3. Causes for the apparent overprediction of BrCl production based on the MECCA chemical scheme are not known, and the potential role of organic matter in halogen activation and multiphase recycling is largely unexplored; laboratory studies are needed to resolve these important areas of uncertainty.

Lastly, the outcome of this study raises broader issues related to model complexity. Specifically, if a model based on a comprehensive chemical mechanism such as MECCA reveals systematic biases in simulated Br cycling, what are the implications for interpreting results of other global model studies of halogens based on less explicit sources and/or reaction mechanisms (e.g., Table 1)? Reactions and respective rate expressions in MECCA are either empirically constrained or based on theoretical estimates of explicit processes (see Sander et al. 2011), and the simplified schemes used in some

other halogen models correspond essentially to subsets of the MECCA mechanism. If causes for bias derive in part from behavior of the chemical mechanism itself and/or parameterization of marine aerosol production, then results based on less comprehensive reaction schemes or similar aerosol production schemes may also be impacted albeit perhaps to differing degrees. Clearly, our study does not yield a more correct result *per se*, and we do not argue that our approach is the correct one in and of itself. It does, however, reveal limitations in the current state of the science at large, both experimental and theoretical, with implications for previous modeling studies. These outstanding issues must be resolved to achieve a reliable understanding of halogen cycling and related implications for Earth systems.

Supplementary material related to this article is available online at <http://www.atmos-chem-phys.net/14/3397/2014/acp-14-3397-2014-supplement.pdf>.

Acknowledgements. The three reviewers and the editor provided constructive suggestions for improving the manuscript. Financial support was provided by the US Department of Energy's (DOE's) Office of Science through the Office of Biological and Environmental Research (BER, grant numbers DE-FG02-07ER64442 and DE-SC0007120 to the University of Virginia), a Global Change Education Program Graduate Research Environmental Fellowship, and the National Center for Computational Sciences at Oak Ridge National Laboratory, which is supported by DOE's Office of Science (BER) under contract DE-AC05-00OR22725. The CESM project is supported by the National Science Foundation and the DOE's Office of Science (BER). PNNL authors were funded by the US Department of Energy, Office of Science, Scientific Discovery through Advanced Computing (SciDAC) program. The Pacific Northwest National Laboratory is operated for DOE by Battelle Memorial Institute under contract DE-AC06-76RLO 1830.

Edited by: B. Ervens

References

- Adams, P. J. and J. H. Seinfeld: Predicting global aerosol size distributions in general circulation models, *J. Geophys. Res.*, 107, 4370, doi:10.1029/2001JD001010, 2002.
- Alexander, B.: Sulfate formation in sea-salt aerosols: Constraints from oxygen isotopes, *J. Geophys. Res.*, 110, D10307, doi:10.1029/2004JD005659, 2005
- Alexander, B., Hastings, M. G., Allman, D. J., Dachs, J., Thornton, J. A., and Kunasek, S. A.: Quantifying atmospheric nitrate formation pathways based on a global model of the oxygen isotopic composition ($\Delta^{17}\text{O}$) of atmospheric nitrate, *Atmos. Chem. Phys.*, 9, 5043–5056, doi:10.5194/acp-9-5043-2009, 2009.
- Allan, W., Lowe, D. C., and Cainey, J. M.: Active chlorine in the remote marine boundary layer: Modeling anomalous measurements of d13C in methane, *Geophys. Res. Lett.*, 28, 3239–3242, 2011.

- Anastasio, C. and Newberg, J. T.: Sources and sinks of hydroxyl radical in sea-salt particles, *J. Geophys. Res.*, 112, D10306, doi:10.1029/2006JD008061, 2007.
- Andreae, M. O. and Rosenfeld, D.: Aerosol-cloud-precipitation interactions. Part 1. The nature and sources of cloud-active aerosols, *Earth Science Reviews*, 89, 13–41, 2008.
- Arimoto, R., Duce, R. A., Savoie, D. L., Prospero, J. M., Talbot, R., Cullen, J. D., Tomza, U., Lewis, N. F., and Jay, B. J.: Relationships among aerosol constituents from Asia and the North Pacific during PEM-West A, *J. Geophys. Res.*, 101, 2011–2023, 1996.
- Birmili, W., Wiedensohler, A., Heintzenberg, J., and Lehmann, K.: Atmospheric particle number size distribution in central Europe: Statistical relations to air masses and meteorology, *J. Geophys. Res.-Atmos.*, 106, 32005–32018, 2001.
- Boville, B. A., Rasch, P. J., Hack, J. J., and McCaa, J. R.: Representation of clouds and precipitation processes in the Community Atmosphere Model Version 3 (CAM3), *J. Climate*, 19, 2184–2198, 2006.
- Breider, T. J., Chipperfield, M. P., Richards, N. A. D., Carslaw, K. S., Mann, G. W., and Spracklen, D. V.: The impact of BrO on dimethylsulfide in the remote marine boundary layer, *Geophys. Res. Lett.*, 37, L02807, doi:10.1029/2009GL040868, 2010.
- Briegleb, B. P., Hunke, E. C., Bitz, C. M., Lipscomb, W. H., Holland, M. M., Schramm, J. L., and Moritz, R. E.: The sea ice simulation of the Community Climate System Model, version 2. Nat. Center for Atm. Res. Tech Rep no. NCAR-TN-455, Boulder, CO, 34 pp., 2004.
- Brown, S. S., Thornton, J. A., Keene, W. C., Pszenny, A. A. P., Sive, B. C., Dubé, W. P., Wagner, N. L., Young, C. J., Riedel, T. P., Roberts, J. M., VandenBoer, T. C., Bahreini, R., Öztürk, F., Middlebrook, A. M., Kim, S., Hübner, G. and Wolfe, D. E.: Nitrogen, Aerosol Composition and Halogens on a Tall Tower (NACHTT): Overview of a wintertime air chemistry field study in the Front Range urban corridor of Colorado, *J. Geophys. Res.-Atmos.*, 118, 8067–8085, doi:10.1002/jgrd.50537, 2013.
- Chameides, W. L. and Stelson, A. W.: Aqueous-phase chemical processes in deliquescent sea-salt aerosols: A mechanism that couples the atmospheric cycles of S and sea salt, *J. Geophys. Res.*, 97, 20565–20580, 1992.
- Clarke, A. D., Owens, S. R., and Zhou, J.: An ultrafine sea salt flux from breaking waves: Implications for cloud condensation nuclei in the remote marine atmosphere, *J. Geophys. Res.*, 111, D06202, doi:10.1029/2005JD006565, 2006.
- Dentener, F., Kinne, S., Bond, T., Boucher, O., Cofala, J., Generoso, S., Ginoux, P., Gong, S., Hoelzemann, J. J., Ito, A., Marelli, L., Penner, J. E., Putaud, J.-P., Textor, C., Schulz, M., van der Werf, G. R., and Wilson, J.: Emissions of primary aerosol and precursor gases in the years 2000 and 1750 prescribed data-sets for AeroCom, *Atmos. Chem. Phys.*, 6, 4321–4344, doi:10.5194/acp-6-4321-2006, 2006.
- Dickerson, R. R., Rhoads, K. P., Carsey, T. P., Oltmans, S. J., Burrows, J. P., and Crutzen, P. J.: Ozone in the remote marine boundary layer: A possible role for halogens, *J. Geophys. Res.*, 104, 21385–21395, 1999.
- Dickinson, R. E., Oleson, K. W., Bonan, G. B., Hoffman, F., Thornton, P., Vertenstein, M., Yang, Z.-L., and Zeng, X.: The Community Land Model and its climate statistics as a component of the Community Climate System Model, *J. Clim.*, 19, 2302–2324, 2006.
- Erickson III, D. J., Seuzaret, C., Keene, W. C., and Gong, S. L.: A general circulation model based calculation of HCl and ClNO₂ production from sea salt dechlorination: Reactive Chlorine Emissions Inventory, *J. Geophys. Res.*, 104, 8347–8372, doi:10.1029/98JD01384, 1999.
- Fickert, S., Adams, J. D., and Crawley, J. N.: Activation of Br₂ and BrCl via uptake of HOBr onto aqueous salt solutions, *J. Geophys. Res.*, 104, 23719–23727, 1999.
- Fitzenberger, R., Bösch, H., Camy-Peyret, C., Chipperfield, M. P., Harder, H., Platt, U., Sinnhuber, B.-M., Wagner, T., and Pfeilsticker, K.: First profile measurements of tropospheric BrO, *Geophys. Res. Lett.*, 27, 2921–2924, 2000.
- Galbally, I. E., Bentley, S. T., and Meyer, C. P.: Mid-latitude marine boundary-layer ozone destruction at visible sunrise observed at Cape Grim, Tasmania, *Geophys. Res. Lett.*, 27, 3841–3844, 2000.
- Gent, P. R., Yeager, S. G., Neale, R. B., Levis, S., and Bailey, D. A.: Improvements in a half degree atmosphere/land version of the CCSM, *Clim. Dynam.*, 34, 819–833, doi:10.1007/s00382-009-0614-8, 2009.
- Granier, C., Guenther, A., Lamarque, J., Mieville, A., Müller, J., Olivier, J., Orlando, J., Peters, J., Petron, G., Tyndall, G., and Wallens, S.: POET, a database of surface emissions of ozone precursors, available at: <http://www.aero.jussieu.fr/projet/ACCENT/POET.php> (last access: 26 March 2014), 2005.
- Gregg, W. W.: Assimilation of SeaWiFS global ocean chlorophyll data into a three-dimensional global ocean model, *J. Marine Syst.*, 69, 205–225, 2008.
- Holmes, C. D., Jacob, D. J., Corbett, E. S., Mao, J., Yang, X., Talbot, R., and Slemr, F.: Global atmospheric model for mercury including oxidation by bromine atoms, *Atmos. Chem. Phys.*, 10, 12037–12057, doi:10.5194/acp-10-12037-2010, 2010.
- Jaeglé, L., Quinn, P. K., Bates, T. S., Alexander, B., and Lin, J.-T.: Global distribution of sea salt aerosols: new constraints from in situ and remote sensing observations, *Atmos. Chem. Phys.*, 11, 3137–3157, doi:10.5194/acp-11-3137-2011, 2011.
- Kamra, A. K.: Measured size distributions of aerosols over the Indian Ocean during INDOEX, *J. Geophys. Res.*, 108, 8000, doi:10.1029/2002JD002200, 2003.
- Keene, W. C., Jacob, D. J., and Fan, S.-M.: Reactive chlorine: A potential sink for dimethylsulfide and hydrocarbons in the marine boundary layer, “New Directins” Commentary, *Atmos. Environ.*, 30, i–iii, 1996.
- Keene, W. C., Sander, R., Pszenny, A. A. P., Vogt, R., Crutzen, P. J., and Galloway, J. N.: Aerosol pH in the marine boundary layer: A review and model evaluation, *J. Aerosol Sci.*, 29, 339–356, 1998.
- Keene, W. C., Stutz, J., Pszenny, A. A. P., Maben, J. R., Fischer, E., Smith, A. M., von Glasow, R., Pechtl, S., Sive, B. C., and Varner, R. K.: Inorganic chlorine and bromine in coastal New England air during summer, *J. Geophys. Res.*, 112, D10S12, doi:10.1029/2006JD007689, 2007.
- Keene, W. C., Long, M. S., Pszenny, A. A. P., Sander, R., Maben, J. R., Wall, A. J., O’Halloran, T. L., Kerkweg, A., Fischer, E. V., and Schrems, O.: Latitudinal variation in the multiphase chemical processing of inorganic halogens and related species over the eastern North and South Atlantic Oceans, *Atmos. Chem. Phys.*, 9, 7361–7385, doi:10.5194/acp-9-7361-2009, 2009.
- Kercher, J. P., Riedel, T. P., and Thornton, J. A.: Chlorine activation by N₂O₅: simultaneous, in situ detection of ClNO₂ and N₂O₅

- by chemical ionization mass spectrometry, *Atmos. Meas. Tech.*, 2, 193–204, doi:10.5194/amt-2-193-2009, 2009.
- Kerkweg, A., Jöckel, P., Pozzer, A., Tost, H., Sander, R., Schulz, M., Stier, P., Vignati, E., Wilson, J., and Lelieveld, J.: Consistent simulation of bromine chemistry from the marine boundary layer to the stratosphere – Part 1: Model description, sea salt aerosols and pH, *Atmos. Chem. Phys.*, 8, 5899–5917, doi:10.5194/acp-8-5899-2008, 2008.
- Kokkola, H., Hommel, R., Kazil, J., Niemeier, U., Partanen, A.-I., Feichter, J., and Timmreck, C.: Aerosol microphysics modules in the framework of the ECHAM5 climate model – intercomparison under stratospheric conditions, *Geosci. Model Dev.*, 2, 97–112, doi:10.5194/gmd-2-97-2009, 2009.
- Kolb, C. E., Cox, R. A., Abbatt, J. P. D., Ammann, M., Davis, E. J., Donaldson, D. J., Garrett, B. C., George, C., Griffiths, P. T., Hanson, D. R., Kulmala, M., McFiggans, G., Pöschl, U., Riipinen, I., Rossi, M. J., Rudich, Y., Wagner, P. E., Winkler, P. M., Worsnop, D. R., and O’Dowd, C. D.: An overview of current issues in the uptake of atmospheric trace gases by aerosols and clouds, *Atmos. Chem. Phys.*, 10, 10561–10605, doi:10.5194/acp-10-10561-2010, 2010.
- Lamarque, J.-F., Bond, T. C., Eyring, V., Granier, C., Heil, A., Klimont, Z., Lee, D., Liouesse, C., Mieville, A., Owen, B., Schultz, M. G., Shindell, D., Smith, S. J., Stehfest, E., Van Aardenne, J., Cooper, O. R., Kainuma, M., Mahowald, N., McConnell, J. R., Naik, V., Riahi, K., and van Vuuren, D. P.: Historical (1850–2000) gridded anthropogenic and biomass burning emissions of reactive gases and aerosols: methodology and application, *Atmos. Chem. Phys.*, 10, 7017–7039, doi:10.5194/acp-10-7017-2010, 2010.
- Lawler, M. J., Finley, B. D., Keene, W. C., Pszenny, A. A. P., Read, K. A., von Glasow, R., and Saltzman, E. S.: Pollution-enhanced reactive chlorine chemistry in the eastern tropical Atlantic boundary layer, *Geophys. Res. Lett.*, 36, L08810, doi:10.1029/2008GL036666, 2009.
- Lawler, M. J., Sander, R., Carpenter, L. J., Lee, J. D., von Glasow, R., Sommariva, R., and Saltzman, E. S.: HOCl and Cl₂ observations in marine air, *Atmos. Chem. Phys.*, 11, 7617–7628, doi:10.5194/acp-11-7617-2011, 2011.
- Leitte, A. M., Schlink, U., Herbarth, O., Wiedensohler, A., Pan, X., Hu, M., Richter, M., Wehner, B., Tuch, T., Wu, Z., Yang, M., Liu, L., Breitner, B., Cyrys, J., Peters, A., Wichmann, H., and Franck, U.: Size-Segregated Particle Number Concentrations and Respiratory Emergency Room Visits in Beijing, China, *Environ. Health Persp.*, 119, 508–513, 2011.
- Lewis, E. R. and Schwartz, S. E.: Sea Salt Aerosol Production: Mechanisms, Methods, Measurements, and Models – A Critical Review, American Geophysical Union., 2004.
- Liu, X., Easter, R. C., Ghan, S. J., Zaveri, R., Rasch, P., Shi, X., Lamarque, J.-F., Gettelman, A., Morrison, H., Vitt, F., Conley, A., Park, S., Neale, R., Hannay, C., Ekman, A. M. L., Hess, P., Mahowald, N., Collins, W., Iacono, M. J., Bretherton, C. S., Flanner, M. G., and Mitchell, D.: Toward a minimal representation of aerosols in climate models: description and evaluation in the Community Atmosphere Model CAM5, *Geosci. Model Dev.*, 5, 709–739, doi:10.5194/gmd-5-709-2012, 2012.
- Long, M. S., Keene, W. C., Kieber, D. J., Erickson, D. J., and Maring, H.: A sea-state based source function for size- and composition-resolved marine aerosol production, *Atmos. Chem. Phys.*, 11, 1203–1216, doi:10.5194/acp-11-1203-2011, 2011.
- Long, M. S., Keene, W. C., Easter, R., Sander, R., Kerkweg, A., Erickson, D., Liu, X., and Ghan, S.: Implementation of the chemistry module MECCA (v2.5) in the modal aerosol version of the Community Atmosphere Model component (v3.6.33) of the Community Earth System Model, *Geosci. Model Dev.*, 6, 255–262, doi:10.5194/gmd-6-255-2013, 2013.
- Mahowald, N. M., Muhs, D. R., Levis, S., Rasch, P. J., Yoshioka, M., Zender, C. S., and Luo, C.: Change in atmospheric mineral aerosols in response to climate: Last glacial period, preindustrial, modern, and doubled carbon dioxide climates, *J. Geophys. Res.*, 111, 10202, doi:10.1029/2005JD006653, 2006.
- Mäkelä, J. M., Koponen, I. K., Aalto, P., and Kulmala, M.: One-year data of submicron size modes of tropospheric background aerosol in southern Finland, *J. Aerosol Sci.*, 31, 595–611, 2000.
- Mårtensson, E. M., Nilsson, E. D., deLeeuw, G., Cohen, L. H., and Hansson, H.-C.: Laboratory simulations and parameterization of the primary marine aerosol production, *J. Geophys. Res.*, 108, 4297, doi:10.1029/2002JD002263, 2003.
- McDow, S. R., Jang, M., Hong, Y., and Kamens R. M.: An approach to studying the effects of organic composition on atmospheric aerosol photochemistry, *J. Geophys. Res.*, 101, 19593–19600, 1996.
- Monahan, E. C. and O’muircheartaigh, I. G.: Whitecaps and the passive remote-sensing of the ocean surface, *Int. J. Remote Sens.*, 7, 627–642, 1986.
- Montzka, S. A., Butler, J. H., Hall, B. D., Mondeel, D. J., and Elkins, J. W.: A decline in tropospheric organic bromine, *Geophys. Res. Lett.*, 30, 1826, doi:10.1029/2003GL017745, 2003.
- Nagao, I., Matsumoto, K., and Tanaka, H.: Sunrise ozone destruction found in the sub-tropical marine boundary layer, *Geophys. Res. Lett.*, 26, 3377–3380, doi:10.1029/1999GL010836, 1999.
- O’Dowd, C. D. and Smith, M. H.: Physico-chemical properties of aerosol over the North East Atlantic: Evidence for wind speed related sub-micron sea-salt aerosol production, *J. Geophys. Res.*, 98, 1137–1149, 1993.
- O’Dowd, C. D., Smith, M. H., Consterdine, I. E., and Lowe, J. A.: Marine aerosol, sea-salt, and the marine sulphur cycle: A short review, *Atmos. Environ.*, 31, 73–80, 1997.
- Ordóñez, C., Lamarque, J.-F., Tilmes, S., Kinnison, D. E., Atlas, E. L., Blake, D. R., Sousa Santos, G., Brasseur, G., and Saiz-Lopez, A.: Bromine and iodine chemistry in a global chemistry-climate model: description and evaluation of very short-lived oceanic sources, *Atmos. Chem. Phys.*, 12, 1423–1447, doi:10.5194/acp-12-1423-2012, 2012.
- Osthoff, H. D., Roberts, J. M., Ravishankara, A. R., Williams, E. J., Lerner, B. M., Sommariva, R., Bates, T. M., Coffman, D., Quinn, P. K., Dibb, J. E., Stark, H., Burkholder, J. B., Talukdar, R. K., Meagher, J., Fehsenfeld, F. C., and Brown, S. S.: High levels of nitryl chloride in the polluted subtropical marine boundary layer, *Nature Geosci.*, 1, 324–328, doi:10.1038/ngeo177, 2008.
- Parrella, J. P., Jacob, D. J., Liang, Q., Zhang, Y., Mickley, L. J., Miller, B., Evans, M. J., Yang, X., Pyle, J. A., Theys, N., and Van Roozendael, M.: Tropospheric bromine chemistry: implications for present and pre-industrial ozone and mercury, *Atmos. Chem. Phys.*, 12, 6723–6740, doi:10.5194/acp-12-6723-2012, 2012.
- Phillips, G. J., Tang, M. J., Thieser, J., Brickwedde, B., Schuster, G., Bohn, B., Lelieveld, J., and Crowley, J. N.: Signifi-

- cant concentrations of nitryl chloride observed in rural continental Europe associated with the influence of sea salt chloride and anthropogenic emissions, *Geophys. Res. Lett.*, 39, L10811, doi:10.1029/2012GL051912, 2012.
- Pierce, J. R. and Adams, P. J.: Global evaluation of CCN formation by direct emission of sea salt and growth of ultrafine sea-salt, *J. Geophys. Res.*, 111, D06203, doi:10.1029/2005JD006186, 2006.
- Piot, M. and von Glasow, R.: The potential importance of frost flowers, recycling on snow, and open leads for ozone depletion events, *Atmos. Chem. Phys.*, 8, 2437–2467, doi:10.5194/acp-8-2437-2008, 2008.
- Platt, U., Allan, W., and Lowe, D.: Hemispheric average Cl atom concentration from $^{13}\text{C}/^{12}\text{C}$ ratios in atmospheric methane, *Atmos. Chem. Phys.*, 4, 2393–2399, doi:10.5194/acp-4-2393-2004, 2004.
- Prospero, J. M., Uematsu, M., and Savoie, D. L.: Mineral aerosol transport to the Pacific Ocean, in: *Chemical Oceanography*, edited by: Ridley, J. P., Chester, R., and Duce, R. A., Elsevier, New York, 188–218, 1989.
- Pszenny, A. A. P., Moldanová, J., Keene, W. C., Sander, R., Maben, J. R., Martinez, M., Crutzen, P. J., Perner, D., and Prinn, R. G.: Halogen cycling and aerosol pH in the Hawaiian marine boundary layer, *Atmos. Chem. Phys.*, 4, 147–168, doi:10.5194/acp-4-147-2004, 2004.
- Pszenny, A. A. P., Fischer, E. V., Russo, R. S., Sive, B. C., and Varner, R. K.: Estimates of Cl atom concentrations and hydrocarbon kinetic reactivity in surface air at Appledore Island, Maine (USA), during International Consortium for Atmospheric Research on Transport and Transformation/Chemistry of Halogens at the Isles of Shoals, *J. Geophys. Res.*, 112, D10S13, doi:10.1029/2006JD007725, 2007.
- Quinn, P. K. and Bates, T. S.: The case against climate regulation via oceanic phytoplankton sulphur emissions, *Nature*, 480, 51–56, doi:10.1038/nature10580, 2011.
- Read, K. A., Majajan, A. S., Carpenter, L. J., Evans, M. J., Faria, B. V. E., Heard, D. E., Hopkins, J. R., Lee, J. D., Moller, S. J., Lewis, A. C., Mendes, L., McQuaid, J. B., Oetjen, H., Saiz-Lopez, A., Pilling, M. J., and Plane, J. M. C.: Extensive halogen mediated ozone destruction over the tropical Atlantic Ocean, *Nature*, 453, 1232–1235, 2008.
- Richter, A., Wittrock, F., Ladstätter-Weißenmayer, A., and Burrows, J. P.: GOME measurements of stratospheric and tropospheric BrO, *Adv. Space Res.*, 29, 1667–1672, 2002.
- Riley, J. P., Chester, R., and Duce, R. A.: Chemical oceanography, Vol. 10, SEAREX : the Sea/Air Exchange Program, edited by: Riley, J. P and Chester, R., Academic Press, New York, 1989.
- Rudolph, J., Koppmann, R., and Plass-Dülmer, C.: The budgets of ethane and tetrachloroethene: Is there evidence for an impact of reactions with chlorine atoms in the troposphere?, *Atmos. Environ.*, 30, 1887–1894, 1996.
- Ruuskanen, J., Tuch, T., Brink, H., Peters, A., Khlystov, A., Mirme, A., Kos, G. P. A., Brunekreef, B., Wichmann, H. E., Buzorius, G., Vallius, M., Kreyling, W. G., and Pekkanen, J.: Concentrations of ultrafine, fine and PM_{2.5} particles in three European cities, *Atmos. Environ.*, 35, 3729–3738, doi:10.1016/S1352-2310(00)00373-3, 2001.
- Saiz-Lopez, A., Plane, J. M. C., and Shillito, J. A.: Bromine oxide in the mid-latitude marine boundary layer, *Geophys. Res. Lett.*, 31, L03111, doi:10.1029/2003GL018956, 2004.
- Saiz-Lopez, A., Lamarque, J.-F., Kinnison, D. E., Tilmes, S., Ordóñez, C., Orlando, J. J., Conley, A. J., Plane, J. M. C., Mahajan, A. S., Sousa Santos, G., Atlas, E. L., Blake, D. R., Sander, S. P., Schauffler, S., Thompson, A. M., and Brasseur, G.: Estimating the climate significance of halogen-driven ozone loss in the tropical marine troposphere, *Atmos. Chem. Phys.*, 12, 3939–3949, doi:10.5194/acp-12-3939-2012, 2012.
- Salawitch, R. J., Canty, T. P., Kurosu, T. P., Chance, K., Liang, Q., Pawson, S., Bhartia, P. K., Liu, X., Huey, L. G., Dibb, J. E., Simpson, W. R., Donohoue, D., Weinheimer, A. J., Flocke, F. M., Newman, J., Nowak, J. B., Ryerson, T. B., Oltmans, S. J., Blake, D. R., Atlas, E. L., Kinnison, D. E., Tilmes, S., Pan, L., Hendrick, F., van Roozendael, M., Kreher, K., Johnston, P. V., Pierce, R., Crawford, J. H., Jacob, D. J., da Silva, A., Nielsen, J. E., Rodriguez, J. M., Liao, J., Stickel, R. E., Tanner, D. J., Knapp, D., Montzka, D., Gao, R. S., Bui, T. P., and Chen, G.: A new interpretation of total column BrO during Arctic spring, *Geophys. Res. Lett.*, 37, L21805, doi:10.1029/2010GL043798, 2010.
- Sander, R.: Modeling atmospheric chemistry: Interactions between gas-phase species and liquid cloud/aerosol particles, *Surv. Geophys.*, 20, 1–31, 1999.
- Sander, R., Rudich, Y., von Glasow, R., and Crutzen, P. J.: The role of BrNO₃ in marine tropospheric chemistry: A model study, *Geophys. Res. Lett.*, 26, 2858–2860, 1999.
- Sander, R., Keene, W. C., Pszenny, A. A. P., Arimoto, R., Ayers, G. P., Baboukas, E., Cainey, J. M., Crutzen, P. J., Duce, R. A., Hönniger, G., Huebert, B. J., Maenhaut, W., Mihalopoulos, N., Turekian, V. C., and Van Dingenen, R.: Inorganic bromine in the marine boundary layer: a critical review, *Atmos. Chem. Phys.*, 3, 1301–1336, doi:10.5194/acp-3-1301-2003, 2003.
- Sander, R., Kerkweg, A., Jöckel, P., and Lelieveld, J.: Technical note: The new comprehensive atmospheric chemistry module MECCA, *Atmos. Chem. Phys.*, 5, 445–450, doi:10.5194/acp-5-445-2005, 2005.
- Sander, R., Baumgaertner, A., Gromov, S., Harder, H., Jöckel, P., Kerkweg, A., Kubistin, D., Regelin, E., Riede, H., Sandu, A., Taraborrelli, D., Tost, H., and Xie, Z.-Q.: The atmospheric chemistry box model CAABA/MECCA-3.0, *Geosci. Model Dev.*, 4, 373–380, doi:10.5194/gmd-4-373-2011, 2011.
- Savoie, D. I., Prospero, J. M., Larsen, R. J., Huang, F., Izaguirre, M. A., Huang, T., Snowdon, T. H., Custals, L., and Sanderson, C. G.: Nitrogen and Sulfur Species in Antarctic Aerosols at Mawson, Palmer Station, and Marsh (King George Island), *J. Atmos. Chem.*, 17, 95–122, 1993.
- Savoie, D. L., Arimoto, R., Keene, W. C., Prospero, J. M., Duce, R. A., and Galloway, J. N.: Marine biogenic and anthropogenic contributions to non-sea-salt sulfate in the marine boundary layer over the North Atlantic Ocean, *J. Geophys. Res.*, 107, 4356, doi:10.1029/2001JD000970, 2002.
- Savoie, D. L., Prospero, J. M., and Saltzman, E. S.: Nitrate, non-seasalt sulfate and methanesulfonate over the Pacific Ocean, in: *Chemical Oceanography*, edited by: Ridley, J. P., Chester, R., and Duce, R. A., Elsevier, New York, 219–250, 1989.
- Schwartz, S. E.: Mass-transport considerations pertinent to aqueous phase reactions of gases in liquid-water clouds, in *Chemistry of Multiphase Atmospheric Systems*, NATO ASI Series, Vol. G6, edited by: Jaeschke, W., 415–471, Springer Verlag, Berlin, 1986.
- Simon, H., Kimura, Y., McGaughey, G., Allen, D. T., Brown, S. S., Osthoff, H. D., Roberts, J. M., Byun, R., and Lee, D.: Modeling

- the impact of ClNO₂ on ozone formation in the Houston area, *J. Geophys. Res.*, 114, D00F03, doi:10.1029/2008JD010732, 2009.
- Simpson, W. R., von Glasow, R., Riedel, K., Anderson, P., Ariya, P., Bottenheim, J., Burrows, J., Carpenter, L. J., Frieß, U., Goodsite, M. E., Heard, D., Hutterli, M., Jacobi, H.-W., Kaleschke, L., Neff, B., Plane, J., Platt, U., Richter, A., Roscoe, H., Sander, R., Shepson, P., Sodeau, J., Steffen, A., Wagner, T., and Wolff, E.: Halogens and their role in polar boundary-layer ozone depletion, *Atmos. Chem. Phys.*, 7, 4375–4418, doi:10.5194/acp-7-4375-2007, 2007.
- Singh, H. B., Gregory, G. L., Anderson, B., Browell, E., Sachse, G. W., Davis, D. D., Crawford, J., Bradshaw, J. D., Talbot, R., Blake, D. R., Thornton, D., Newell, R., and Merrill, J.: Low ozone in the marine boundary layer of the tropical Pacific Ocean: Photochemical loss, chlorine atoms, and entrainment, *J. Geophys. Res.*, 101, 1907–1917, 1996.
- Sommariva, R. and von Glasow, R.: Multiphase Halogen Chemistry in the Tropical Atlantic Ocean, *Environ. Sci. Technol.*, 46, 10429–10437, doi:10.1021/es300209f, 2012.
- Spracklen, D. V., Pringle, K. J., Carslaw, K. S., Chipperfield, M. P., and Mann, G. W.: A global off-line model of size-resolved aerosol microphysics: I. Model development and prediction of aerosol properties, *Atmos. Chem. Phys.*, 5, 2227–2252, doi:10.5194/acp-5-2227-2005, 2005.
- Stanier, C. O., Khlystov, A. Y., and Pandis, S. N.: Ambient aerosol size distributions and number concentrations measured during the Pittsburgh Air Quality Study (PAQS), *Atmos. Environ.*, 38, 3275–3284, 2004.
- Stutz, J., Thomas, J. L., Hurlock, S. C., Schneider, M., von Glasow, R., Piot, M., Gorham, K., Burkhardt, J. F., Ziembka, L., Dibb, J. E., and Lefer, B. L.: Longpath DOAS observations of surface BrO at Summit, Greenland, *Atmos. Chem. Phys.*, 11, 9899–9910, doi:10.5194/acp-11-9899-2011, 2011.
- Tanaka, P. L., Riemer, D. D., Chang, S. H., Yarwood, G., McDonald-Buller, E. C., Apel, E. C., Orlando, J. J., Silva, P. J., Jimenez, J. L., Canagaratna, M. R., Neece, J. D., Mullins, C. B., and Allen, D. T.: Direct evidence for chlorine-enhanced urban ozone formation in Houston, Texas, *Atmos. Environ.*, 37, 1393–1400, 2003.
- Textor, C., Schulz, M., Guibert, S., Kinne, S., Balkanski, Y., Bauer, S., Berntsen, T., Berglen, T., Boucher, O., Chin, M., Dentener, F., Diehl, T., Easter, R., Feichter, H., Fillmore, D., Ghan, S., Ginoux, P., Gong, S., Grini, A., Hendricks, J., Horowitz, L., Huang, P., Isaksen, I., Iversen, I., Kloster, S., Koch, D., Kirkevåg, A., Kristjansson, J. E., Krol, M., Lauer, A., Lamarque, J. F., Liu, X., Montanaro, V., Myhre, G., Penner, J., Pitari, G., Reddy, S., Seland, Ø., Stier, P., Takemura, T., and Tie, X.: Analysis and quantification of the diversities of aerosol life cycles within AeroCom, *Atmos. Chem. Phys.*, 6, 1777–1813, doi:10.5194/acp-6-1777-2006, 2006.
- Theye, N., Van Roozendael, M., Hendrick, F., Yang, X., De Smedt, I., Richter, A., Begoin, M., Errera, Q., Johnston, P. V., Kreher, K., and De Mazière, M.: Global observations of tropospheric BrO columns using GOME-2 satellite data, *Atmos. Chem. Phys.*, 11, 1791–1811, doi:10.5194/acp-11-1791-2011, 2011.
- Thornton, J. A., Kercher, J. P., Riedel, T. P., Wagner, N. L., Cozic, J., Holloway, J. S., Dubé, W. P., Wolfe, G. M., Quinn, P. K., Middlebrook, A. M., Alexander, B., and Brown, S. S.: A large atomic chlorine source inferred from mid-continental reactive nitrogen chemistry, *Nature*, 464, 271–274, doi:10.1038/nature08905, 2010.
- Toumi, R.: BrO as a sink for dimethylsulfide in the marine atmosphere, *Geophys. Res. Lett.*, 21, 117–120, 1994.
- Vogt, R., Crutzen, P. J., and Sander, R.: A mechanism for halogen release from sea-salt aerosol in the remote marine boundary layer, *Nature*, 383, 327–330, 1996.
- von Glasow, R. and Crutzen, P. J.: Model study of multiphase DMS oxidation with a focus on halogens, *Atmos. Chem. Phys.*, 4, 589–608, doi:10.5194/acp-4-589-2004, 2004.
- von Glasow, R., Sander, R., Bott, A., and Crutzen, P. J.: Modeling halogen chemistry in the marine boundary layer. 2. Interactions with sulfur and cloud-covered MBL, *J. Geophys. Res.*, 107, 4323, doi:10.1029/2001JD000943, 2002.
- von Glasow, R., von Kuhlmann, R., Lawrence, M. G., Platt, U., and Crutzen, P. J.: Impact of reactive bromine chemistry in the troposphere, *Atmos. Chem. Phys.*, 4, 2481–2497, doi:10.5194/acp-4-2481-2004, 2004.
- Wingenter, O. W., Kubo, M. K., Blake, N. J., Smith Jr., T. W., Blake, D. R., and Rowland, F. S.: Hydrocarbon and halocarbon measurements as photochemical and dynamical indicators of atmospheric hydroxyl, atomic chlorine, and vertical mixing obtained during Lagrangian flights, *J. Geophys. Res.*, 101, 4331–4340, 1996.
- Wingenter, O. W., Blake, D. R., Blake, N. J., Sive, B. C., Atlas, E., Flocke, F., and Rowland, F. S.: Tropospheric hydroxyl and atomic chlorine concentrations, and mixing time scales determined from hydrocarbon and halocarbon measurements made over the Southern Ocean, *J. Geophys. Res.*, 104, 21819–21828, 1999.
- Yang, X., Cox, R. A., Warwick, N. J., Pyle, J. A., Carver, G. D., O'Connor, F. M., and Savage, N. H.: Tropospheric bromine chemistry and its impacts on ozone: A model study, *J. Geophys. Res.*, 110, D23311, doi:10.1029/2005JD006244, 2005.
- Young, A. H., Keene, W. C., Pszenny, A. A. P., Sander, R., Thornton, J. A., Riedel, T. P., and Maben J. R.: Phase partitioning of soluble trace gases with size-resolved aerosols in near-surface continental air over northern Colorado, USA during winter, *J. Geophys. Res.-Atmos.*, 118, 9414–9427, doi:10.1002/jgrd.50655, 2013.
- Zhou X., Davis, A. J., Kieber, D. J., Keene, W. C., Maben, J. R., Maring, H., Dahl, E. E., Izaguirre, M. A., Sander, R., and Smoydzyn, L.: Photochemical production of hydroxyl radical and hydroperoxides in water extracts of nascent marine aerosols produced by bursting bubbles from Sargasso seawater, *Geophys. Res. Lett.*, 35, L20803, doi:10.1029/2008GL035418, 2008.